Mesoscale and Radar Observations of the Fort Collins Flash Flood of 28 July 1997

Walter A. Petersen,* Lawrence D. Carey,* Steven A. Rutledge,* Jason C. Knievel,* Nolan J. Doesken,*,+ Richard H. Johnson,* Thomas B. McKee,*,+ Thomas Vonder Haar,*,# and John F. Weaver@

ABSTRACT

On the evening of 28 July 1997 the city of Fort Collins, Colorado, experienced a devastating flash flood that caused five fatalities and over 200 million dollars in damage. Maximum accumulations of rainfall in the western part of the city exceeded 10 in. in a 6-h period. This study presents a multiscale meteorological overview of the event utilizing a wide variety of instrument platforms and data including rain gauge, CSU–CHILL multiparameter radar, Next Generation Radar, National Lightning Detection Network, surface and Aircraft Communication Addressing and Reporting System observations, satellite observations, and synoptic analyses.

Many of the meteorological features associated with the Fort Collins flash flood typify those of similar events in the western United States. Prominent features in the Fort Collins case included the presence of a 500-hPa ridge axis over northeastern Colorado; a weak shortwave trough on the western side of the ridge; postfrontal easterly upslope flow at low levels; weak to moderate southwesterly flow aloft; a deep, moist warm layer in the sounding; and the occurrence of a quasi-stationary rainfall system. In contrast to previous events such as the Rapid City or Big Thompson floods, the thermodynamic environment of the Fort Collins storm exhibited only modest instability, consistent with low lightning flash rates and an absence of hail and other severe storm signatures.

Radar, rain gauge, and lightning observations provided a detailed view of the cloud and precipitation morphology. Polarimetric radar observations suggest that a coupling between warm-rain collision coalescence processes and ice processes played an important role in the rainfall production. Dual-Doppler radar and mesoscale wind analyses revealed that the low-level flow field associated with a bow echo located 60 km to the southeast of Fort Collins may have been responsible for a brief easterly acceleration in the low-level winds during the last 1.5 h of the event. The enhanced flow interacted with both topography and the convection located over Fort Collins, resulting in a quasi-stationary convective system and the heaviest rainfall of the evening.

*Department of Atmospheric Science, Colorado State University, Fort Collins, Colorado.
+Colorado Climate Center, Department of Atmospheric Science, Colorado State University, Fort Collins, Colorado.
#Cooperative Institute for Research in the Atmosphere, Colorado State University, Fort Collins, Colorado.
@NOAA/NESDIS, RAMM Branch, Cooperative Institute for Research in the Atmosphere, Colorado State University, Fort Collins, Colorado.
Corresponding author address: Dr. Walter A. Petersen, Department of Atmospheric Science, Colorado State University, Fort Collins, CO 80523.
E-mail: walt@olympic.atmos.colostate.edu
In final form 19 August 1998.

1. Introduction

On the evening of 28 July 1997 the city of Fort Collins, Colorado, experienced a devastating flash flood that caused five fatalities and greater than 200 million dollars in damage. The rainfall associated with this event set new records in Fort Collins (FCL) for the largest 1-day, 6-h, and 3-h precipitation totals recorded at the Colorado State University (CSU) weather observatory, and is one of the largest rainfall events ever documented over a developed urban area in Colorado (Doesken and McKee 1998). At the CSU observatory, 5.30 in. (13.46 cm) of rain fell in just

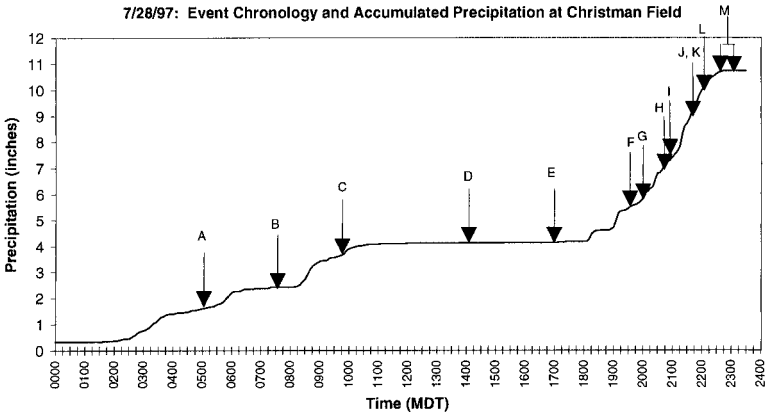

FIG. 1. Chronology of events for 28 July 1997 vs accumulated precipitation (inches) at Christman Field (cf. Fig. 3). Time (MDT) is indicated on the abscissa. Events labeled A–M are discussed in section 1a.

under 6 h. By comparison, the Fort Collins 100-yr 6-h and 24-h rainfall amounts as indicated in the National Oceanic and Atmospheric Administration (NOAA) Atlas-2 (Miller et al. 1973) are 3.50 and 4.80 in., respectively. Approximately 4 km southwest of the CSU weather station, a maximum of 10.2 in. of rain was recorded by a gauge in a 6-h period.

a. Event chronology

The FCL flood was the result of a series of rain events that occurred over a 30-h period ending in an extremely heavy downpour on the evening of 28 July. A chronology of events beginning at 0000 MDT (mountain daylight time) on 28 July 1997 is presented in Fig. 1 relative to a time series of rainfall measured at Christman Airport in northwestern FCL (cf. Figs. 2–3). Earlier, on the evening of 27 July, up to 2.42 in. of rain fell in the foothills immediately west and northwest of FCL (Fig. 2). These rains were followed in the early morning of 28 July (e.g., 0300–1000 MDT; Fig. 1) by another episode of heavy rain on the west side of FCL, extending into the foothills and to the northwest of the city. At 0500 MDT on 28 July ("A" in Fig. 1) the National Weather Service (NWS) in Denver, Colorado, issued a special weather statement outlining the potential for heavy rains and flash flooding in and along the foothills of the northern Colorado Front Range in association with the development of moist low-level upslope flow and weak upper-level winds (cf. section 4). By 0730 MDT ("B" in Fig. 1) flooding had occurred in parts of Laporte and in locations northwest of Laporte (cf. Fig. 3) where 7–9 in. of rain had fallen. As moderate to heavy rain continued to fall along the foothills, the NWS issued an urban and small stream flood advisory (USF) at 0940 MDT ("C"; Fig. 1). The rainfall along the foothills west and northwest of FCL ended around 1200 MDT, and at 1400 MDT the USF was canceled ("D"; Fig. 1). However, as the afternoon progressed, heavy rainfall redeveloped over the central and northern foothills west and northwest of FCL (Fig. 2), leading to the issuance of a flash flood watch at 1700 MDT ("E" in Fig. 1).

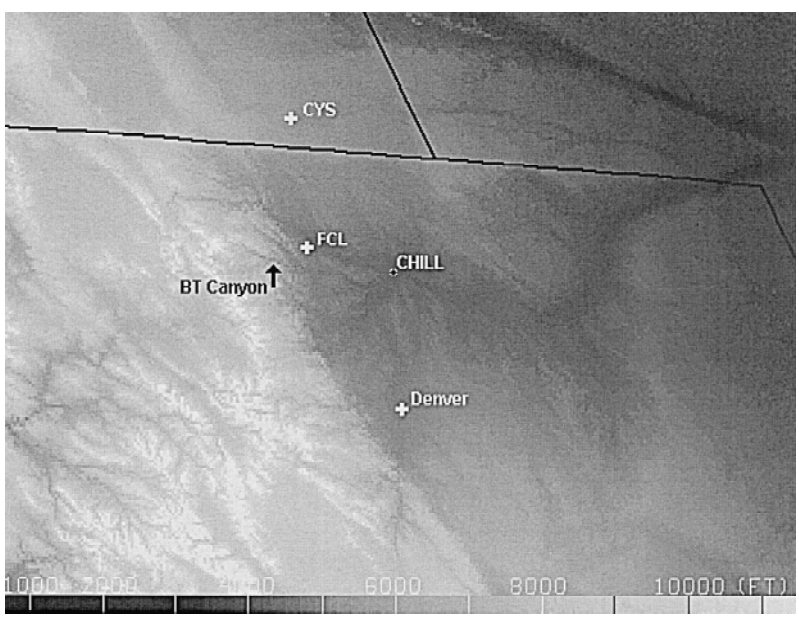

FIG. 2. Map of regional topography with the locations of Fort Collins, CSU–CHILL, Cheyenne, Denver, and the Big Thompson canyon indicated. Elevation intervals (ft) are shaded as indicated at the bottom of the figure.

Between 1700 and 2000 MDT, two small convective systems moved over FCL producing brief heavy rains (e.g., 0.5–0.75 in. of rain in 30 min) before moving off to the north-northeast of the city. During the second rain episode (1900–1930 MDT; Fig. 1), the NWS issued a USF for FCL (1936 MDT; "F" in Fig. 1). Following issuance of the USF, a third area of heavy rain moved over the city from the southwest between 2000 and 2030 MDT and remained quasi-stationary over the western side of

FCL until approximately 2230 MDT. As the rainfall began to increase after 2000 MDT, surface runoff forced the closing of several streets in western FCL and the opening of the FCL Emergency Operations Center ("G" in Fig. 1). Between 2100 and 2200 MDT, the rainfall became especially heavy, exceeding 4–5 in. per hour in some locations. Previously saturated soil coupled with urban surface runoff turned city streets, canals, and creeks into fast-moving torrents of water. Surface water converged on the campus of CSU ("I" in Fig. 1) and began to flood streets, and later, buildings. By 2134 MDT ("J" in Fig. 1) homes in southwestern FCL began to flood and a flash flood warning was issued by the NWS at 2140 MDT ("K" in Fig. 1).

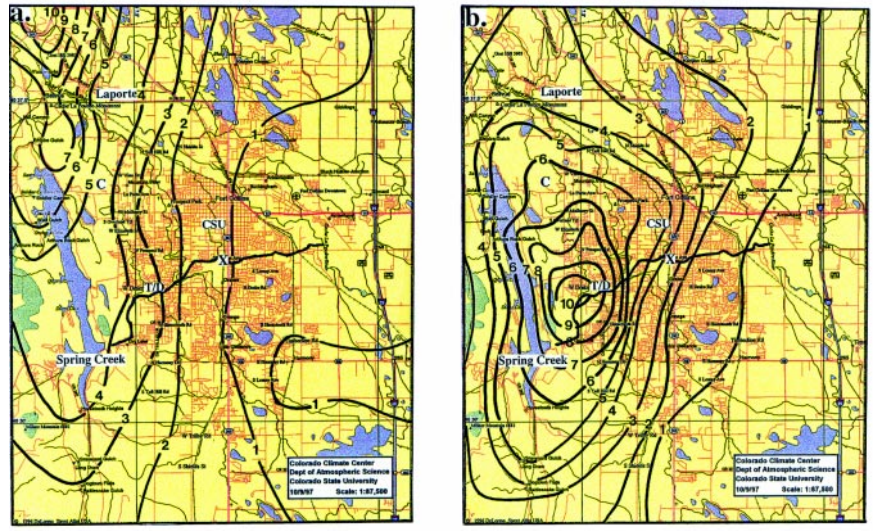

FIG. 3. Isohyetal maps of rainfall for FCL, contoured in inches: (a) 1600 MDT 27 July 1997–1300 MDT 28 July 1997; and (b) 1730–2300 MDT 28 July 1997. The location of Spring Creek is highlighted by a bold line that extends from western FCL at the marker "Spring Creek" through the "X" in central FCL. Locations of the CSU weather station and Christman Field are indicated by "CSU" and "C", respectively. The intersection of Taft Hill and Drake Roads (cf. Fig. 9) is indicated by "T/D", and the approximate locations of the ruptured culvert and flooded mobile home park are indicated by an "X". Figure adapted from Doesken and McKee (1998).

Spring Creek, a small stream that flows east through southern and central FCL (cf. Fig. 3) began to overflow a major city street in southwestern FCL near 2045 MDT ("H" in Fig. 1), and one hour later (2200; "L" in Fig. 1) it was over its banks in western and south-central FCL. In south-central FCL, a 50-acre detention pond located behind a railroad berm briefly contained the combined overflow of Spring Creek and other drainages (cf. Weaver et al. 1998). However, between 2230 and 2300 MDT ("M" in Fig. 1) the detention area reached its 4.6×10^5 m^3 capacity and began to overflow (Weaver et al. 1998). Hydrostatic pressure ruptured a culvert built into the railroad berm, sending the previously detained water directly into a mobile home park located on the eastern side of the berm. In what could only be described as unfortunate timing, a freight train ("M" in Fig. 1) passed over the same area at approximately 2300 MDT and was subsequently derailed by the flooding. Tragically, five people were killed during this time period, and the mobile home park and many businesses were completely destroyed. Preliminary estimates of the peak discharge along Spring Creek on the night of the flood exceeded 6000 cfs in at least two locations, and in many locations were nearly twice that of the "500-year flood" discharge.[1]

b. Meteorological data

On the night of the flood a variety of instrumentation and observations provided extensive meteorological sampling of the FCL storm and the synoptic environment. The observational database and instrumentation (see Fig. 2 for relative locations) included two NWS Next Generation Weather Radar (NEXRAD) Doppler radars located in Denver, Colorado (KFTG; 100 km southeast of FCL), and Cheyenne, Wyoming (KCYS; 70 km northeast of FCL); the CSU–CHILL dual-polarized S-band radar (40 km east-southeast of FCL); 251 rain gauges operated by citizens and public institutions in the vicinity of FCL; the National Lightning Detection Network (NLDN); surface mesonet stations; and geostationary satellite platforms (e.g., *GOES-8*, -9). These observations were combined with ancillary datasets such as wind profiler, sounding, Aircraft Communication Addressing and Reporting System (ACARS), synoptic observations/analyses, and numerical model output. This extensive dataset provides an opportunity to study the

[1]City of FCL, Office of Emergency Management [http://www.ci.fort-collins.co.us/C_SAFETY/OEM//index.htm].

meteorological conditions associated with a flash flood over many spatial and temporal scales.

In the following sections we present a meteorological overview of the FCL flood. First, a discussion of the climatology of extreme rainfall events in Colorado is presented in section 2. Section 3 discusses rain gauge data and presents accumulated rainfall totals for the entire 2-day event (e.g., 27–28 July 1997), as well as the 6-h time period encompassing the flash flood. Section 4 presents an overview of the synoptic environment, followed in section 5 by a presentation of surface mesoanalyses. Section 6 summarizes the preconditioning of the large-scale environment and subsequent triggering of convection over FCL. Multiparameter and dual-Doppler radar observations including radar estimates of accumulated rainfall are described in section 7.

2. Climatology of extreme rain events in Colorado

The Fort Collins flood occurred in a synoptic environment that is commonly associated with severe weather in northeastern Colorado (Doswell 1980), and during a time of year when extreme weather events are expected in northeastern Colorado (Weaver and Doesken 1990). Indeed, even in the semiarid climate of Colorado, extreme rainfall events with local totals exceeding 4 in. in less than 24 h occur several times each year somewhere in the state. However, storms producing greater than 10 in. of rain are rare. A recent climatological investigation of extreme precipitation events in Colorado (McKee and Doesken 1997) showed a distinct tendency for the largest events recorded during the twentieth century to occur at or near the eastern base of the Rocky Mountains, extending from the lower foothills eastward onto the western fringe of the Great Plains. Prior to July of 1997, there had been seven documented storms this century that produced at least 10 in. of rain within 24 h. Several other Front Range storms have produced excessive rainfall but at lower rates and over longer periods of time. For example, an early May storm in 1969 produced close to 15 in. of precipitation over a 4-day period in the mountains and foothills immediately northwest of Denver (Fig. 2). The most publicized of Colorado's extreme rainfall events is the Big Thompson storm (e.g., Maddox et al. 1978; Caracena et al. 1979) of 31 July 1976 (Fig. 2), a canyon flash flood that resulted in 139 confirmed fatalities and a list of seven additional missing persons (Gruntfest 1996).

Based on an examination of more than 300 of Colorado's heaviest precipitation events since the late 1800s, the vast majority of these events were found to occur between mid-April and mid-October but with a double peaked distribution. The first peak occurs late in May and early June, associated with synoptic-scale quasi-stationary late spring storms. These storms carry moisture from the Gulf of Mexico and the Mississippi Valley westward to the Front Range of the Rockies (Fig. 2), where it typically falls as widespread precipitation of moderate intensity with localized convective and orographic enhancement. The maximum precipitation from these storms is typically found along the eastern foothills of the Rockies. A distinct lull in the frequency of extreme rainfall events occurs from late June into July. This is followed by the second and greater peak in storm frequency from late July extending into early September with a pronounced maximum frequency from the last week of July into the first few days of August. These summer storms are highly convective, often small in areal extent, and have occurred in nearly all parts of Colorado. However, the greatest of these, in terms of maximum rainfall, have occurred east of the mountains and often near the eastern foothills of the Rockies. The FCL storm of 28 July 1997 fits very neatly within this climatological description.

3. Rain gauge measurements of accumulated rainfall for the FCL flood

Immediately following the 27–28 July FCL events, the Colorado Climate Center began an extensive effort to document the rainfall (e.g., Figs. 3a,b). Using radio, newspaper, and broadly distributed electronic mail requests in combination with traditional door-to-door and phone surveys, rainfall reports were solicited from all possible sources. In all, more than 300 rainfall reports were gathered, 90% of which were based on rain gauge measurements. As much information as possible was gathered for each rain report including gauge type, exposure, observing procedures, latitude and longitude of the gauge location, and any additional human observations to supplement the gauge measurements. Upon completion of data gathering activities, gauge locations and amounts deemed highly reliable (110 reports for the night of 28 July; 209 reports for the two-day event, 27–28 July) were plotted on a map

and an isohyetal analysis was performed (e.g., Figs. 3a,b). To extend the rain gauge analysis on the extreme western edge of the city where rain gauge data were sparse, radar rainfall estimates (CSU–CHILL and NEXRAD) were used to quantitatively adjust the overall pattern of the precipitation isohyets. This was accomplished in a two-step process. First, the ratio of rain gauge to CSU–CHILL radar-estimated rainfall (cf. section 7b) over the gauge sites was determined (and found to be nearly constant). Next, radar-estimated rainfall totals for multiple grid points located on the western side of FCL were multiplied by the ratio and the isohyetal analysis was completed.

A key component of the investigation was the collection of recording rain gauge data to document the timing and intensity of rainfall. While no systematic network of recording rain gauges existed in the FCL area, a total of 14 recording gauges were located in the immediate vicinity, a few with 1-min time resolution and 0.01-in. resolution. The data from these gauges provided the necessary information to deduce the timing of rainfall events, thus greatly facilitating the interpretation of the manual measurements, some of which were single storm accumulations and others that were measurements for specific time periods during the storm.

Observed rainfall patterns for two periods are shown in Figs. 3a,b. The total rainfall from the late afternoon of 27 July through midday 28 July is shown in Fig. 3a. Most of the city of FCL recorded between 0.6 and 2 in. during this period. However, as much as 4 in. of rain fell over the far western part of FCL, and more than 9 in. of rain fell over a small area 12.8 km northwest of the center of FCL and immediately northwest of the town of Laporte. Rainfall accumulations from the evening of the flash flood (28 July) are shown in Fig. 3b. The observed rainfall accumulations for this 5.5-h period exceeded 10 in. over extreme southwestern FCL (and over Spring Creek in particular; Fig. 3b) and were in excess of 6 in. over most portions of western FCL. A striking rainfall gradient was present to the southeast of the point of maximum precipitation, where rainfall totals decreased from 10 in. to less than 2 in. in a distance of only 4 km.

4. The synoptic environment

a. Midtroposphere

Expansive high pressure lay over the west-central United States during the final days of July 1997 as evinced by the presence of a ridge with an axis that extended from the Mississippi Delta to the Pacific Northwest (Fig. 4). Within the western periphery of the ridge was a shortwave trough extending from Nevada into southern Wyoming. At the western side of the trough was a maximum in vorticity over the border of Nevada and Utah; the maximum had moved northwestward from its original location in south-central Utah 12 h earlier. The eastern part of the trough had a weak and narrow arm of vorticity extending into southern Wyoming, according to the Nested Grid Model initializations at 0600 and 1800 MDT (not shown). The easterly wind at Lander, Wyoming, is consistent with positive vorticity north of the shortwave trough in Colorado, away from the site of the flood.

Light to moderate[2] southern and southwesterly winds advected a deep layer of moisture into Colorado (Fig. 4) along the spine of the southern Rocky Mountains. Dewpoint depressions at 500 hPa were 1°C at all sounding sites in New Mexico, Colorado, and Wyoming (Fig. 4). Overall, the main synoptic features aloft resembled those that accompanied the 1972 Rapid City and 1976 Big Thompson (hereafter referred to as RC and BT) flash floods (Maddox et al. 1978; Caracena et al. 1979).

On the night of the flood, storms from Denver to FCL developed at about the same time that a cluster of relatively cold cloud tops crossed the northern Front Range after having traveled north-northeastward from central New Mexico within the monsoonal flow. A 12-h series of the cluster's footprints, as determined from Geostationary Operational Environmental Satellite (*GOES-8*) infrared imagery, is shown in Fig. 5. The northernmost footprint in Fig. 5 depicts the perimeter of these cloud tops at 1800 MDT, just prior to the onset of flooding rains in FCL and coincident with strengthening convection located in the Denver area that shortly thereafter evolved into a bow echo (cf. sections 5, 6). Whether or not the cold cloud tops were dynamically linked with the shortwave trough mentioned earlier is unclear.

b. Surface

At the surface, a cool and exceptionally moist Canadian air mass was lodged against the eastern face

[2]Although the 500-hPa analysis from the National Centers for Environmental Prediction depicts winds of 2.5–10 m s^{-1} over the southern Rockies, data from the ACARS indicate winds in the upper troposphere approached 23 m s^{-1} just south of Fort Collins at about 1800 MDT 28 July (Fig. 6).

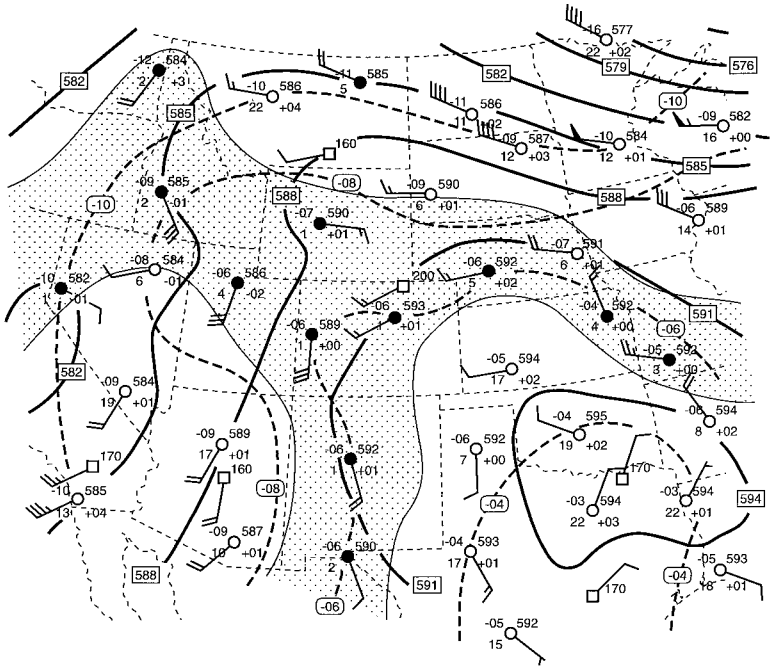

FIG. 4. 500-hPa analysis for 1800 MDT 28 July 1997 (0000 UTC 29 July 1997). Isolines of geopotential height (solid) are contoured at an interval of 30 m. Isotherms (dashed) are contoured at an interval of 2°C. Shaded regions indicate dewpoint depressions ≤ 6°C.

of the Rockies in Colorado and Wyoming (e.g., 1800 MDT 28 July 1997; Fig. 5). Dewpoints were 16°–18°C (61–64°F) along the foothills and 18°–20°C a few hundred kilometers to the east. The slow-moving cool front that led the Canadian air mass was located almost 700 km to the south in northeastern New Mexico and northern Texas (Fig. 5). In northeastern Colorado and southeastern Wyoming, anticyclonic flow from the Canadian air mass produced northeasterly to southeasterly winds of 2.5–8 m s^{-1} over the high plains. This synoptic pattern is also similar to those observed for the RC and BT storms (Maddox et al. 1978), with one important exception: the surface front in the case of the FCL storm was located much farther south of the flood area than were the fronts associated with the RC and BT cases.

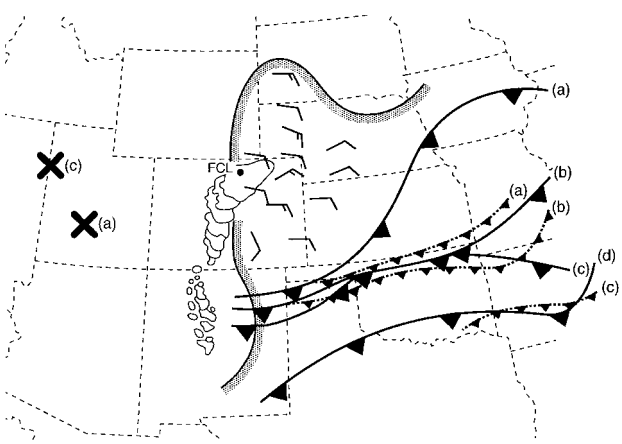

FIG. 5. Schema of synoptic and mesoscale features for 28 July 1997. Two large Xs represent the locations of a 500-hPa vorticity maximum. Closed solid contours indicate pertinent regions of cloud top colder than –20°C for 1-h intervals between 0600 and 1800 MDT. The wide shaded line shows the northwestern edge of surface dewpoints > 15.5°C (60°F). Wind barbs are for the surface; short barbs are 2.5 m s^{-1}, long barbs are 5 m s^{-1}. Synoptic fronts are indicated by solid lines; mesoscale boundaries by broken lines with pairs of dots. Times are (a) 0600, (b) 1200, (c) 1800, and (d) 2400 MDT.

c. Soundings

The nearest sounding to FCL was taken by the NWS at Denver (DNR, 85 km south-southeast of FCL) at 1800 MDT on 28 July (Fig. 6). In an attempt to infer conditions closer to FCL, we have included a vertical profile of temperature and wind transmitted via the Aircraft Communication Addressing and Reporting System (Benjamin et al. 1991). The 14 wind and temperature measurements that compose the ACARS sounding were taken within ±1 h of 1800 MDT and within a circle defined by FCL at the center and DNR at the perimeter; this ensured that the aircraft data were at least as near to the flooded area as was the sonde launch site. The ACARS sounding is broadly consistent with the DNR sounding, with a few exceptions. Lower temperatures from 400 to 500 hPa in the ACARS sounding may reflect aircraft penetrations of clouds. Further, the ACARS winds were much stronger than the sonde winds from 300 to 400 hPa, perhaps because of mesoscale variability and local storms.

The third sounding in Fig. 6 depicts the mean vertical temperature profile of the atmosphere overlying the tropical western Pacific warm pool as calculated from soundings made within the intensive flux array during the intensive observing period of the Tropical Ocean and Global Atmosphere Coupled Ocean–Atmosphere Response Experiment (TOGA COARE). The remarkable similarity between the TOGA COARE sounding and those from near FCL attests to the tropical nature of the environment that fostered the flash flood.

The DNR sounding shows very moist conditions throughout the troposphere, with no lower-tropospheric inversion or cap above the boundary layer. Midtropospheric winds were weak to moderate and southwesterly, and winds from the surface to 750 hPa were east to southeasterly. The total precipitable water below 500 hPa at DNR was 3.4 cm; the July average is 1.9 cm and values exceed 2.8 cm only 5% of the time. The soundings proximate to the RC and BT storms exhibited similarly high values of precipitable water (Maddox et al. 1978; Caracena et al. 1979).

Table 1 lists some of the thermodynamic variables calculated from the DNR sounding. Note that the thermodynamic parameters were relatively insensitive to methods of mixing the boundary layer and to inclusion of surface conditions at Fort Collins. A very shallow isothermal layer existed from near the surface to 810 hPa. The troposphere was conditionally unstable from 810 to 500 hPa and from 460 to 400 hPa. Convective available potential energy (CAPE) was relatively small at 868 J kg^{-1} (assuming pseudoadiabatic ascent of a parcel with the mean thermodynamic characteristics of the lowest 1 km of the sounding). The relatively small negative lifted index of −2.8 also indicates only a slightly unstable troposphere. The modest instability of the troposphere prior to the FCL flood differs markedly from the highly unstable profiles of the RC and BT floods, for which the lifted indices were −7 and −6, respectively (Maddox et al. 1978; Caracena et al. 1979). The small dewpoint depressions for the FCL storm produced a low lifting condensation level (LCL) of 764 hPa and a low level of free convection (LFC) of 690 hPa. The 0°C level in the DNR sounding was located at a height of approximately 3.6 km above ground level (AGL) (570 hPa).

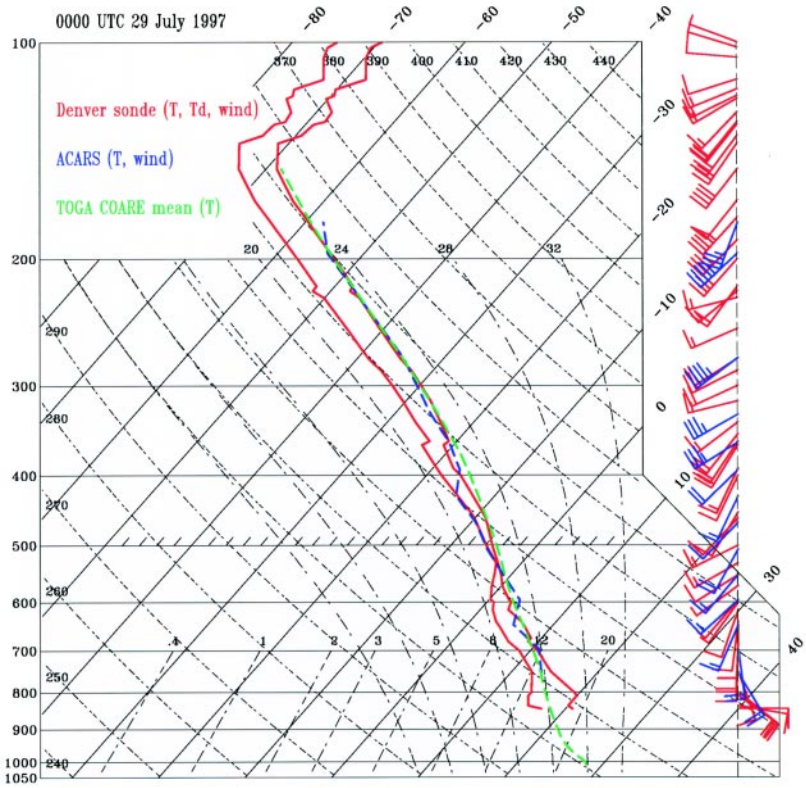

FIG. 6. Skew-*T* plot for Denver, CO, at 1800 MDT and for TOGA COARE (see text). The respective soundings are labeled in the upper left corner of the figure. Wind barbs are plotted in knots; full wind barb = 10 kt (5 m s^{-1}), half barb = 5 kt (2.5 m s^{-1}).

TABLE 1. Denver sounding characteristics.

Precipitable water through 500 hPa (% climatology)	3.4 cm (179%)
Precipitable water through 100 hPa	3.8 cm
Lifting condensation level (LCL)	764 hPa
Level of free convection (LFC)	690 hPa
Environmental 0°C level	570 hPa
CAPE	868 J kg^{-1}
Lifted index	−2.8

5. Surface mesoanalyses

Surface streamline mesoanalyses from 1800 to 2100 MDT 28 July 1997 are shown in Figs. 7 a–d. The analyses are based on National Weather Service, Colorado Agricultural Meteorological, and Colorado Department of Transportation surface stations. Positions of outflow boundaries are based on radar data and surface observations (e.g., wind shifts, temperature drops).

For most of the afternoon of 28 July the surface flow field over northeastern Colorado resembled that

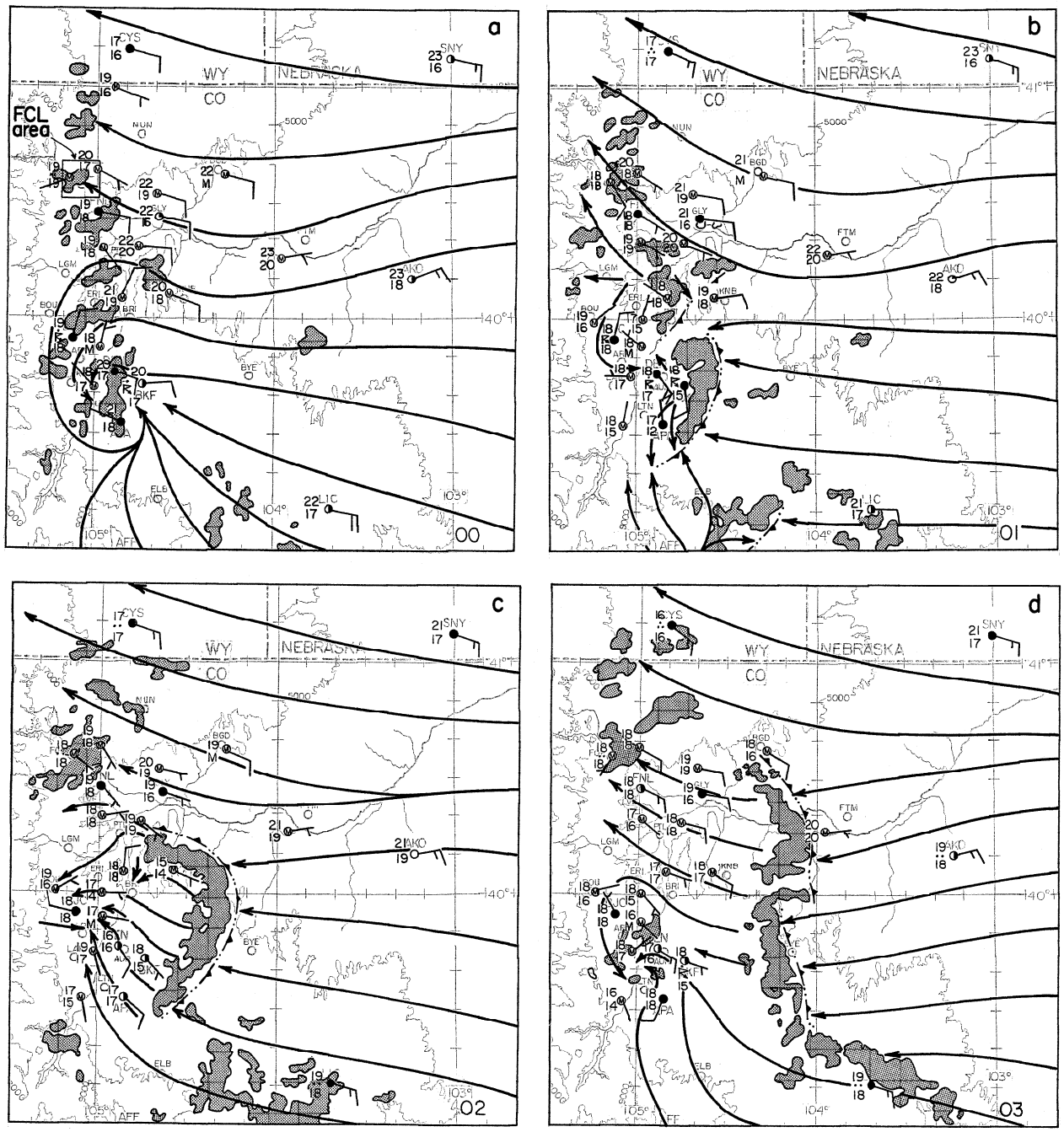

FIG. 7. Hourly mesoscale analyses for 1800–2100 MDT 28 July 1997 (0000–0300 UTC 29 July 1997). Surface streamlines are in solid arrows. Wind barbs plotted as in Fig. 6; temperature and dewpoints in °C. Mesoscale boundaries are indicated as in Fig. 5. Regions of radar reflectivity ≥ 35 dB*Z* are shaded: (a) 1800 (0000), (b) 1900 (0100), (c) 2000 (0200), and (d) 2100 MDT (0300 UTC).

shown in Fig. 7a. Generally east-to-southeasterly flow prevailed over the Front Range, except in the vicinity of Denver, where a Denver cyclone was evident. This cyclonic circulation commonly develops when southeasterly flow impinges on the Palmer Lake Divide (Szoke et al. 1984; Blanchard and Howard 1986; Brady and Szoke 1989). Its formation has been attributed to a variety of mechanisms (see Davis 1997 for a review). This convergence associated with the Denver Cyclone (e.g., Wilczak and Christian 1990) appears to have played a role in initiating a bow echo in the Denver area after 1800 MDT, which then moved onto the plains at 8 m s^{-1} over the next 3 h (Figs. 7a–d). However, the bow echo was also coincident with

the passage over the Denver area of the long-lived convective feature traceable in infrared satellite imagery all the way back to central New Mexico (Fig. 5).

The development of the bow echo in the weakly sheared environment illustrated in Figs. 7c–d is partially consistent with modeling simulations discussed by Weisman and Davis (1998). The Weissman and Davis study indicates that bow echoes can develop in environments of weak vertical wind shear (e.g., 10 m s^{-1}/2.5 km) where there is large CAPE (2500–4500 J kg^{-1}). However, such values of CAPE well exceed those associated with the environment of the FCL flood (868 J kg^{-1}). The bow echo in this case did not produce the strong surface winds that are often associated with such phenomena (Przbylinski 1995). It did, however, exhibit a rear-inflow jet and weak circulation features that resembled bookend vortices (a lower-tropospheric cyclonic circulation on the north end and an anticyclonic circulation on the south; confirmed by dual-Doppler observations and discussed in section 7b) consistent with previous studies of bow echoes (Fujita 1978; Weisman 1993).

During the 4-h period represented in Figs. 7a–d there is a remarkable contrast between the convection to the south of FCL, characterized by the mobile bow echo, and that over FCL, characterized by quasi-stationary convection. What accounted for this difference is unclear. However, convergence associated with the Denver cyclone and the convective feature visible on infrared satellite imagery (Fig. 5) crossing the Denver area from the southwest may have helped to initiate the transitory convective phenomenon in the Denver area. The flow in the FCL area was not influenced by the Denver cyclone as it arrived unimpeded by this topographic circulation throughout the period of the flood. However, it does appear to have been influenced somewhat by the bow echo that passed to the south. Comparison of analyses at 2000 and 2100 MDT (Figs. 7c–d) indicates an acceleration of the east-southeasterly flow between these two times, apparently in response to the surface downdraft outflow behind the bow echo. Further, winds in the immediate vicinity of FCL became more easterly during this period, implying an increase in the component of the flow normal to the north–south-oriented foothills just west of FCL. These changes increased the moisture flux into the FCL area at approximately the same time that the third, and heaviest, rainfall episode developed (Fig. 1).

6. The roles of preconditioning and triggering in the storm environment

Surface upslope flow was the primary preconditioner for the FCL storm because the high humidity associated with the easterly winds meant that relatively little lifting was necessary to raise boundary layer air to its LFC at 690 hPa (compared to an LFC of 620 hPa for the BT storm; Caracena et al. 1979). Unlike the BT storm, where a front combined with orographic lift provided the primary trigger for convection (Caracena et al. 1979), the only apparent[3] trigger for the initial area of convection associated with the FCL storm was the foothills. For example, considering only the easterly component of the wind profile (approximately orthogonal to the foothills) presented in Fig. 6, it can be inferred that the lowest 1–1.5 km of the troposphere would have been lifted upon encountering the foothills west of FCL (Fig. 2). This situation contrasts somewhat with the BT flood; namely, the lower LFC in the FCL case would have permitted generation of heavy rainfall as the flow reached its first pronounced orographic lift on the west side of FCL. Of course, it is too simplistic to think of forcing throughout the storm only in terms of the foothills orography. It is likely that other factors such as outflow boundaries (which played a role in cell initiation near FCL later in the event; cf. section 7), latent and sensible heating gradients, and pressure perturbations also played roles in the distribution of convection and heavy rainfall along the Front Range.

In the few hours before the flood, the wind profiler in Platteville, Colorado (about 45 km southeast of FCL), registered a 5–8 m s^{-1} wind that veered from southeasterly to southerly over the lowest 2 km of the troposphere. Satellite-derived cloud-drift wind vector fields (at approximately 1 km AGL) were calculated from *GOES-9* visible imagery for two periods on 28 July (1400–1423 and 1700–1723 MDT; Figs. 8a,b) using three images per period. Consistent with the wind profiler data, at 1416 MDT (Fig. 8a) the cloud-drift winds also indicate the presence of a 5 m s^{-1} low-level southeasterly wind. However, at 1715 MDT (Fig. 8b) the cloud-drift winds suggest that the winds backed slightly, becoming more east-southeasterly and increasing in speed by 5 m s^{-1}. The increase in upslope flow over the plains of northeastern Colorado (also

[3]The nearest resolvable front was almost 700 km south when the Fort Collins storm developed. It is possible that a proximate boundary did exist but was not apparent in the conventional observations.

a)

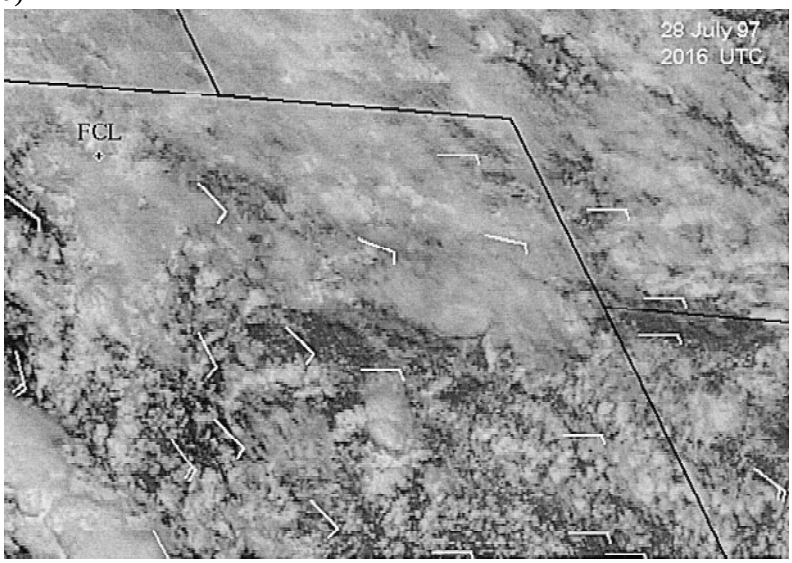

b)

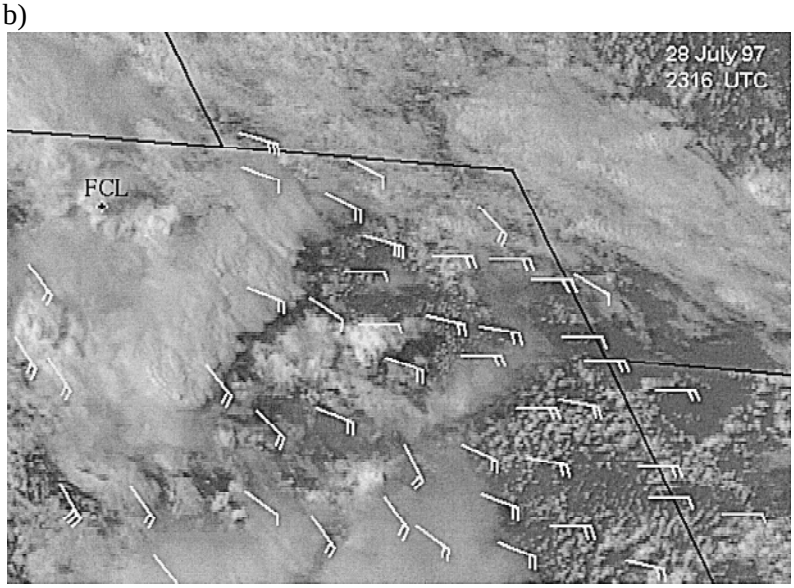

FIG. 8. Cloud drift winds derived from *GOES-9*, 28 July 1997: (a) 2016 (1416) and (b) 2315 UTC (1715 MDT). Winds barbs are plotted in knots; half barb = 5 kt (2.5 m s^{-1}), full barb = 10 kt (5 m s^{-1}). The location FCL is indicated.

observed in the BT case; e.g., Caracena et al. 1979) was nearly coincident with an increase in convection along the northern and central sections of the Front Range (Fig. 8a,b) and just prior to the first pulse of rainfall over the FCL area (e.g., Fig. 1).

Numerous precursors in the storm environment shaped the character and motion of the convection, including a warm, moist south-southwesterly flow above the boundary layer, a low-level east-southeasterly wind, a relatively low CAPE and LFC, and high humidity through the depth of the sounding. The moist monsoonal flow likely promoted high precipitation efficiencies due to minimal entrainment of dry air with its associated evaporation in developing convection. Further, the depth of the "warm" layer between the cloud base (~700 m AGL) and the freezing level (~3.6 km AGL) was nearly 3 km, facilitating the production of rainfall via warm-rain collision–coalescence. Once formed, high boundary layer humidities coupled with low cloud bases likely prevented substantial evaporation of precipitation below cloud base.

Additionally, the Fort Collins storm formed in a region characterized by 1) focusing mechanisms for convection such as orography and outflow interactions; 2) a veering wind profile between the surface and 3 km; 3) moderate southwesterly flow aloft (Fig. 6); and 4) low-level advection of moist, high-θ_e air by an increasing upslope flow (Figs. 8a,b). From a convective organization viewpoint, these factors led to an environment that was highly conducive to the development of "training" convection (cf. section 7a) and the development of a quasi-stationary rainfall system (e.g., Miller 1978; Chappell 1986; Doswell et al. 1996).

7. Radar observations

Data collected by the KCYS–NEXRAD (closest NEXRAD to FCL; 5-min volume scans; VCP-11 mode) and the CSU–CHILL (dual-polarized volume scans, 5–15-min intervals) radars were used to document 3D precipitation structure, evolution of the low-level mesoscale wind field (1-km height level), and to create storm total rainfall maps using a variety of radar rainfall estimators for comparison to the rain gauge data (e.g., Fig. 3b).

a. Overview of storm evolution on the evening of 28 July 1997

The first two episodes of heavy rainfall on the evening of 28 July 1997 occurred between 1800 and 2000 MDT (e.g., Fig. 1) in association with two small

(20 km × 20 km) groups of northward-moving convective cells, which were separated in time by approximately 1–1.5 h. The final and heaviest period of rainfall occurred over FCL between 2000 and 2215 MDT in association with convection originally located along the foothills southwest of FCL that moved north-northeast and eventually became quasi stationary over the city.

Constant Altitude Plan Position Indicators (CAPPIs), constructed from KCYS reflectivity data and covering approximately the last two hours of the flood event, are presented in Figs. 9a–i. These figures emphasize heavily raining convection located directly over FCL, with the origin of the coordinate system located at the intersection of Taft Hill and Drake Roads. Note that the area of moderate to heavy rain (reflectivities ≥ 40 dB*Z*) in each of the panels is relatively small, and that the maximum reflectivities (55–58 dB*Z*) are not out of the ordinary for a typical summertime thunderstorm over the northeastern plains of Colorado.

Several spatial and temporal features of the precipitation that were highly relevant to the resultant flooding can be discerned in Fig. 9. Near 2000 MDT (Fig. 9a), the final round of heavy rain developed over the already saturated ground of southwestern and central FCL. As time progressed, convective elements in the northern part of the storm continued to move slowly toward the north-northeast, dissipating as they moved north of town (e.g., Figs. 9c–f). However, the southern extension of the convection continually regenerated west of FCL over both the foothills and a weak outflow boundary (Fig. 10). The outflow boundary (x = –7–1; y = –3–0; Fig. 10) was generally confined to levels ≤ 1 km AGL, but created a zone of convergence and new cell growth on the south-southeastern flank of the storm where the ambient east-southeasterly flow ($V_r > 0$) encountered the westerly component ($V_r < 0$) of the outflow (e.g., Fig. 13; x = 0, y = –1.5). Once initiated, the new cells moved northeastward (~220° at 6–8 m s^{-1}) and down the Spring Creek basin, producing heavy rainfall as they merged with the larger echo mass.

Between 2030 and 2100 MDT, and coincident with new cell development occurring on the southern and southeastern flanks of the storm, the echo area contracted in size (heavy rainfall became concentrated in an area ≤ 10 × 10 km^2), increased in intensity, and became quasi stationary over southwestern FCL (Figs. 9e–i; Fig. 10). The area contraction of the storm, most evident in the radar imagery after 2100 MDT (e.g., Figs. 9e–i), is consistent with visual observations of the convection taken east of FCL around 2030 MDT. These observations describe the storm clouds as "originally spreading northeastward, but then condensing into a small but ominous cloud mass over and west of the city" (Doesken and McKee 1998). After 2100 MDT (Fig. 9e), heavy rainfall possessing maximum reflectivities of 58 dB*Z* (indicated by the CSU–CHILL) and core diameters on the order of 1–2 km continued to form on the southern and southeastern flanks of the storm and move toward the northeast, *directly down the Spring Creek drainage* (e.g., Figs. 9e–i). This pattern of cell regeneration, movement, and merger over a given location has been observed in many previous flash flood events (Caracena et al. 1979; Miller 1978, Chappell 1986; Smith et al. 1996; Doswell et al. 1996). The production of new convective cells ceased over FCL at approximately 2215 MDT (not shown), and the rainfall stopped shortly thereafter (around 2230 MDT).

There was no hail or severe weather (strong winds, tornado, or funnel clouds, etc.) reported or detected in association with the storm. Further, in contrast to several previous studies of flash flood events that have noted copious amounts of cloud-to-ground (CG) lightning (e.g., Holle and Bennet 1997; Bauer-Messmer et al. 1997; Soula et al. 1998), only 20 CG lightning flashes were detected by the NLDN in the vicinity of FCL over the 5-h duration of the event (Fig. 11; cf. section 7c). During the final two hours of the storm, a period associated with 4–6 in. of rainfall (≥ 50% of the 6-h total), only 7 CGs were detected by the NLDN. Lightning (Fig. 11), radar (e.g., Figs. 8a–d), and satellite imagery (e.g., Fig. 8b) all indicated the presence of larger, more intense areas of convection to the southeast of FCL. Indeed, when viewed instantaneously and on a regional scale (e.g., Fig. 7), the convection located over FCL on the night of 28 July 1997 was rather innocuous in appearance.

b. Dual-Doppler observations of the horizontal wind field

Surface mesoscale analyses presented in section 5 provided a regional view of the low-level horizontal flow field evolution. Interestingly, the mesoscale streamline analyses (Figs. 7c–d) suggest that surface easterly winds increased in magnitude between 2000 and 2100 MDT near and to the southeast of FCL, coincident with the northeastward movement of a band of convection originally situated to the south of FCL. The relatively coarse resolution of the surface wind data in the mesoanalysis makes it difficult to isolate the role that the increase in easterly wind had on the

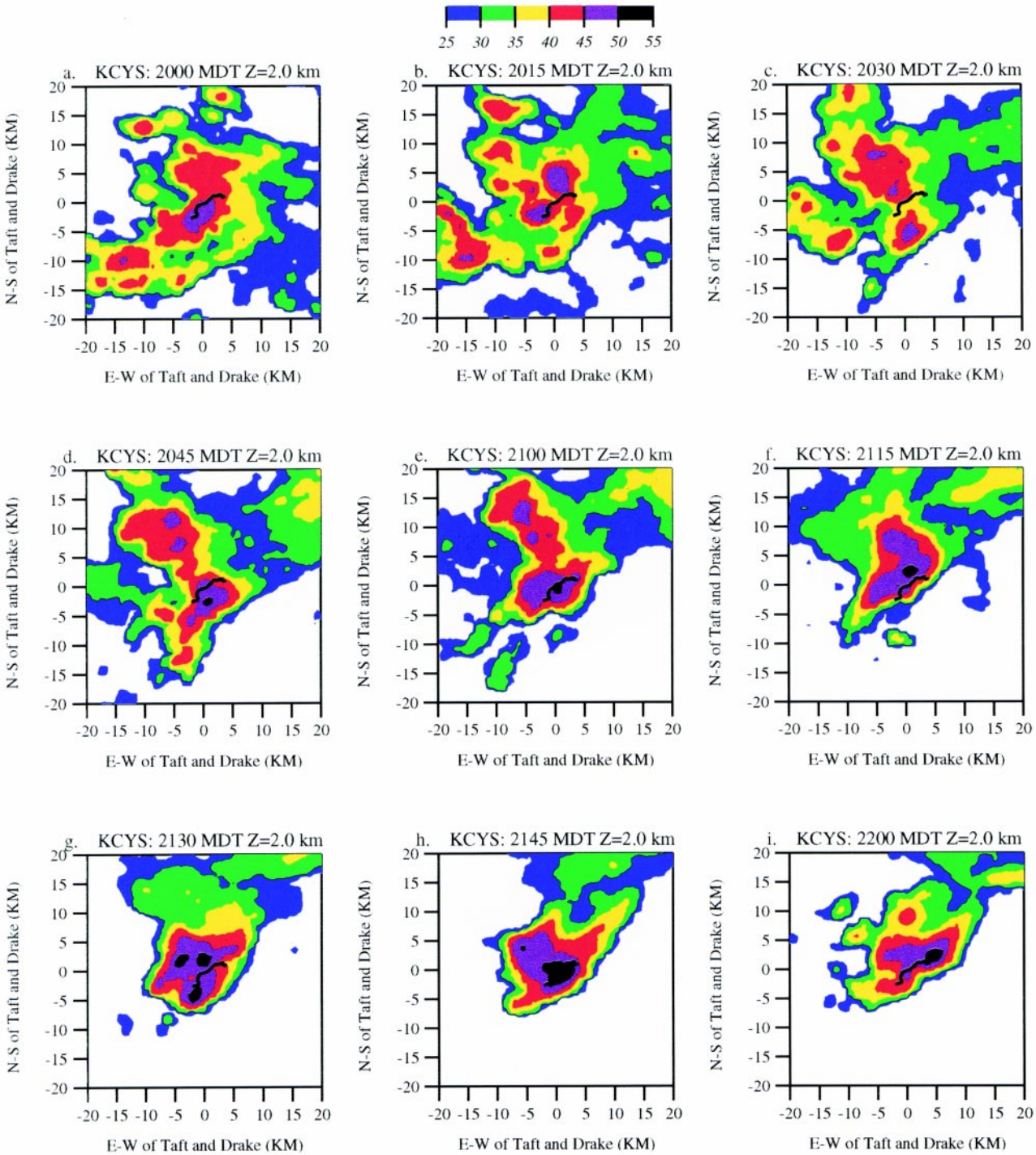

FIG. 9. CAPPIs of radar reflectivity (Z = 2 km) from the KCYS NEXRAD radar for 2000–2200 MDT 28 July 1997. The grid origin (0, 0) is centered on the intersection of Taft Hill and Drake Road in FCL (cf. Fig. 3). A portion of Spring Creek is indicated by the bold line that begins near its headwaters, nearly intersects the origin, and ends just east of the "X" location shown in Fig. 3: (a) 2000, (b) 2015, (c) 2030, (d) 2045, (e) 2100, (f) 2115, (g) 2130, (h) 2145, and (i) 2200 MDT.

small area of convection located over FCL. Indeed, given a finer temporal and spatial resolution, one question that analysis of the low level wind-field could address is, why did the third pulse of convection over southwestern FCL become stationary and intensify during the *last* 1.5 h of the event (e.g., Figs. 9e–i)? For example, if system motion can be represented as a vector sum of cell movement and system propagation

due to a new cell growth (e.g., Chappell 1986), how might changes in the low-level flow have affected the sum of these two vectors in the vicinity of FCL to produce zero net storm movement?

Availability of Doppler radar data from the CSU–CHILL and KCYS–NEXRAD radars facilitated an examination of the coevolving horizontal wind field and precipitation structure using combined radial velocity estimates in a dual-Doppler synthesis (Figs. 12a,b). Due to the 80-km baseline between CSU–CHILL and KCYS, the 70-km distance between KCYS and FCL, and beam curvature/refractivity considerations, the lowest level for which horizontal winds could be synthesized was 1 km. Reflectivity and radial velocity data for both radars were interpolated to a Cartesian grid using a horizontal (vertical) spacing of 2 (1) km; then the two-dimensional wind field was computed for the 1-km height level using CEDRIC software (Mohr and Miller 1983). Note that *only* the horizontal winds were computed in the dual-Doppler synthesis, and *only* the 1-km level will be discussed in this study. No attempt was made to compute vertical velocity due to the long baseline and incomplete sampling of cloud tops by CSU–CHILL (maximum elevation angle 8°).

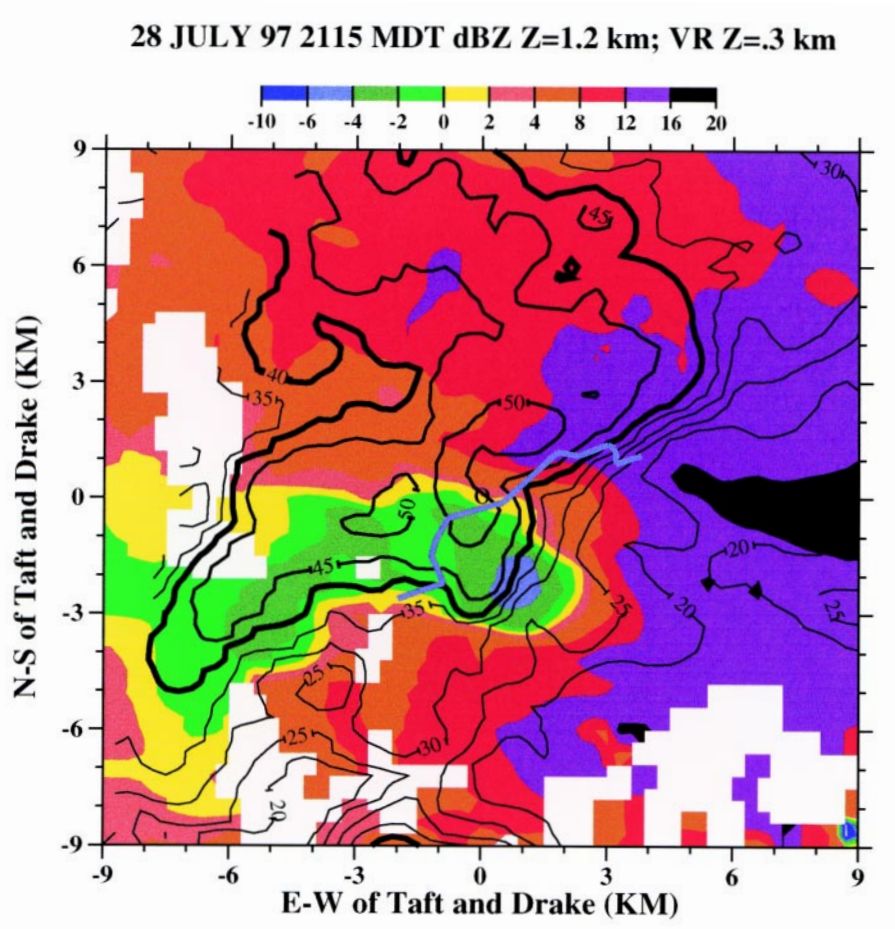

FIG. 10. CSU–CHILL 2115 MDT 28 July 1997: radial wind velocity (shaded in m s^{-1}) at 300-m AGL and radar reflectivity (1.2 km AGL) contoured every 5 dBZ, beginning at 20 dBZ. The CSU–CHILL radar is located at an azimuth of 116° and ~40–45 km from the origin (as in Fig. 9). Warm colors indicate outbound radial velocities (~easterly, southeasterly), cool colors indicate inbound (~westerly) radial velocities. A portion of Spring Creek is also indicated by the bold blue line running through the origin. Note that wind data are missing on the west side of the figure where elevated terrain is located.

Perhaps the most intriguing result of the dual-Doppler analysis is the apparent influence of a bow echo system (located 60–80 km southeast of FCL; Figs. 12a,b) on the mesoscale flow field affecting convection located over western FCL.[4] Prior to 2000 MDT, radar-measured winds in the vicinity of FCL were southeasterly at the 1-km level (consistent with winds near the 750-hPa level in Fig. 6). However, after 2000 MDT scattered convection located along the foothills of the Front Range to the south of FCL (Figs. 7a–d) began to organize and move slowly northeastward, taking the form of a bow echo (e.g., Fujita 1978; Weissman 1993; Weissman and Davis 1998). Dual-Doppler analyses (e.g., Figs. 12a,b) suggest that the low-level winds backed slightly in an area located along and to the west of the northern edge of the bow echo system (e.g., Figs. 12a,b, X = 40–60, Y = –20–5 and X = 0–15, Y = 5–10) as it passed to the southeast of the CSU–CHILL radar. The change in low-level flow forced by the bow echo, combined with inflow associated with the convection over FCL, resulted in a narrow ribbon of flow dominated by an enhanced easterly wind component that terminated in convection located over Spring Creek (Fig. 13).

[4]In the storm-relative framework of the bow echo (not shown), a cyclonic vortex existed on the northern end of the bow echo, with a weaker, but discernible anticyclonic vortex located on the southern end.

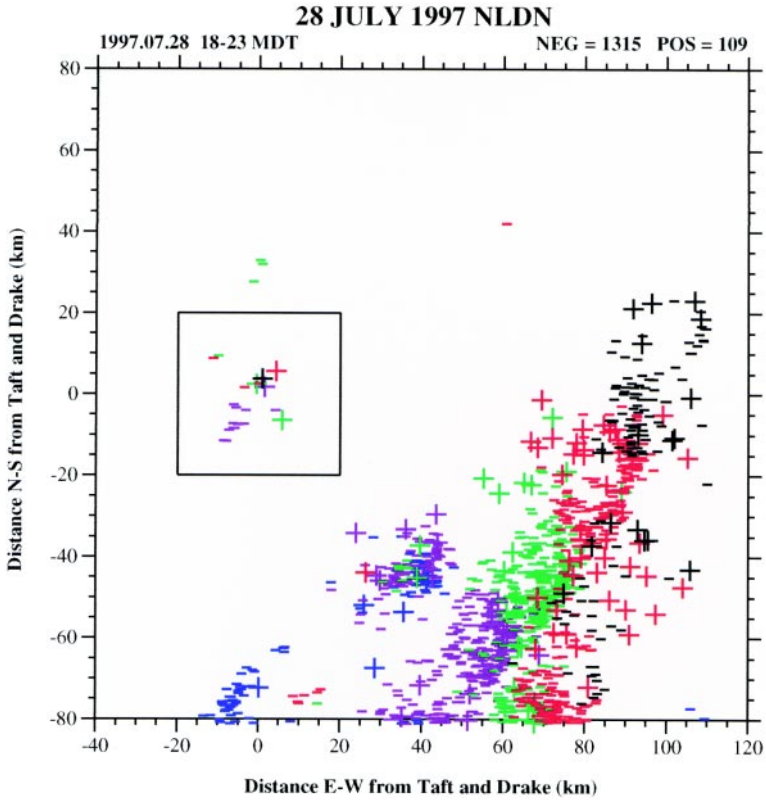

FIG. 11. Cloud-to-ground lightning detected between 1800 and 2300 MDT on 28 July 1997. Grid origin as in Fig. 9. Colors represents CG flash locations detected in 1-h intervals: 1800–1900 (blue), 1900–2000 (purple), 2000–2100 (green), 2100–2200 (red), and 2200–2300 MDT (black). The locations of negative and positive polarity CG flashes are indicated by a (–) and (+), respectively. The CG flash counts by polarity are indicated in the upper-right corner of the figure. The small box embedded within the larger grid encloses the area plotted in Fig. 9.

Radar reflectivity data (Figs. 9d–i) indicate that the last group of convective cells and heavy rainfall began to stall over southwestern FCL after 2030 MDT, nearly coincident with the onset of increased low-level east-southeasterly flow. To further illustrate the relationship between the increased easterly wind component and the onset of heavy convective rainfall after 2030 MDT, a time series (2032–2215 MDT) of line-averaged easterly wind speeds and the relative deviation of those speeds from the value at 2032 MDT was computed utilizing the dual-Doppler analyses. The mean easterly wind components were computed along a 25 km long north–south-oriented line, located at x = 15 and extending from y = 10–15 in Fig. 12. The relative deviation and mean of the easterly wind component for each time was then overlaid on a time series of rain mass flux for the FCL storm computed from CSU–CHILL polarimetric radar data (cf. section 7d). The resultant time series (Fig. 14) exhibits a high positive correlation (r = 0.91) between the easterly wind and rain mass flux after 2030 MDT, consistent with the hypothesis that local enhancements in the easterly wind resulted in a corresponding increase in heavy rainfall over FCL. Caracena et al. (1979) noted a similar correlation between changes in the easterly flow and corresponding changes in rainfall for the BT flood.

The resultant quasi-stationary nature of the storm during the last 1.5 h of the event appeared to be the result of an increase in the magnitude of the system propagation vector, which, in the net, extended toward the south-southwest. The appearance of new cells and heavy rain along the southern flank of the storm was likely the result of interaction between the enhanced, moist east-southeasterly flow, a weak low-level outflow boundary (Fig. 10), and local topography (Fig. 2). Hence, the sum of cell movement and system propagation vectors resulted in a quasi-stationary storm (e.g., Miller 1978; Chappell 1986).

c. Combined polarimetric and NEXRAD observations of storm vertical structure

Observations of deep convection using dual-polarized radar have provided new insights into the microphysical and electrical development of convective clouds (e.g., Goodman et al. 1988; Bringi et al. 1997; Jameson et al. 1996; Ramachandran et al. 1996; Carey and Rutledge 1996, 1998). Combinations of multiparameter variables such as differential reflectivity (Z_{DR}), specific differential phase (K_{DP}), and linear depolarization ratio (LDR) provide information on hydrometeor size, shape, and thermodynamic phase (the presence of oblate raindrops, hail, melting, etc.; cf. Jameson and Johnson 1990; Doviak and Zrnic 1993), thereby reducing the ambiguities involved with inferring cloud microphysical properties based solely on radar reflectivity (Z).

For example, Z_{DR} is the ratio (expressed in dB) of reflectivity measured at horizontal polarization (Z_H) to that of vertical polarization and provides information on the reflectivity-weighted mean hydrometeor axis ratio. The presence of large, oblate particles (e.g., large raindrops) tends to increase the Z_{DR} from near zero to several decibels. The K_{DP} (expressed in degrees

per kilometer) is proportional to the product of the mass-weighted hydrometeor axis ratio and the precipitation liquid water content (Jameson 1985), and is derived from the range derivative of the differential propagation phase between vertically and horizontally polarized radiation. Also, K_{DP} tends to increase from 0° km^{-1} to several degrees per kilometer in regions of substantial precipitation liquid water content. Qualitatively, LDR provides information on the hydrometeor phase, shape, and orientation by measuring the relative amount of depolarized power (in dB) returned from scatterers in a given radar pulse volume. Pulse volumes with mixtures of liquid water and ice (e.g., mixed phase) or canted, irregularly shaped particles all act to increase the LDR. In the case of the FCL flood, Z_{DR}, K_{DP}, and LDR were collected by the CSU–CHILL radar and when combined with reflectivity and CG lightning data, provide insight into the microphysical characteristics of the flood convection.

To set the framework for discussion of the polarimetric observations, first consider the time–height series of KCYS mean radar reflectivity computed for a *stationary* cylindrical volume (10-km radius, 14-km height) centered on Taft Hill and Drake Roads in FCL, shown in Fig. 15 (28 July 1997 1725–2225 MDT). Note that Fig. 15 also includes a time series of rain mass flux (CSU–CHILL radar estimate; see section 7d) and marks indicating the time of occurrence of individual CG lightning flashes. Three primary pulses in convective rainfall separated in time by approximately 1–1.5 h are apparent in Fig. 15 (peaks at minutes 85, 155, 260). The life cycle of

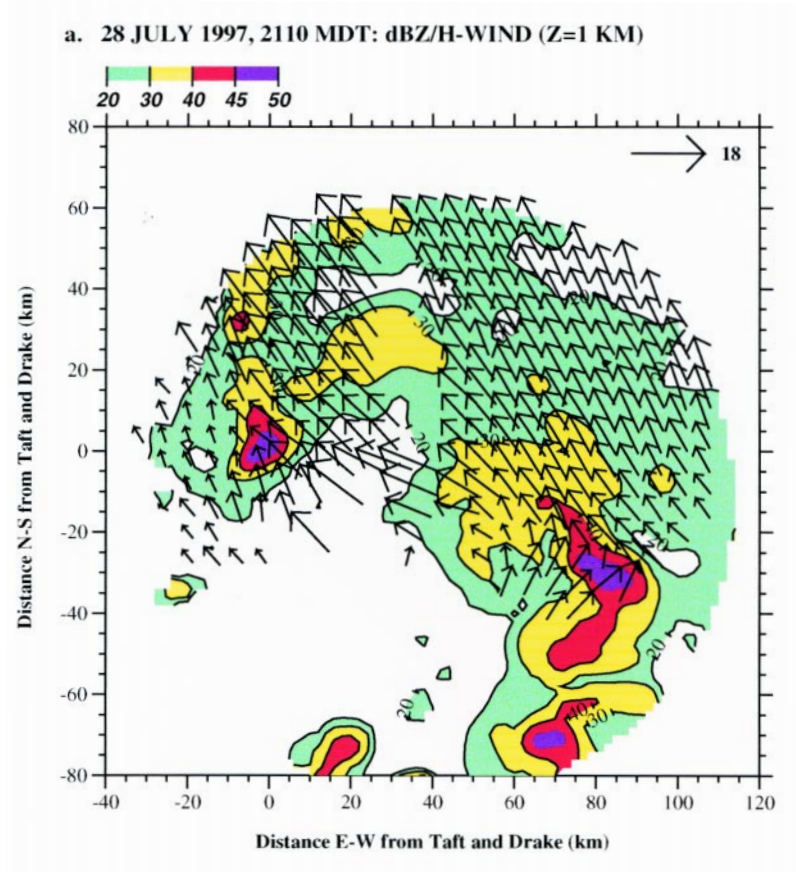

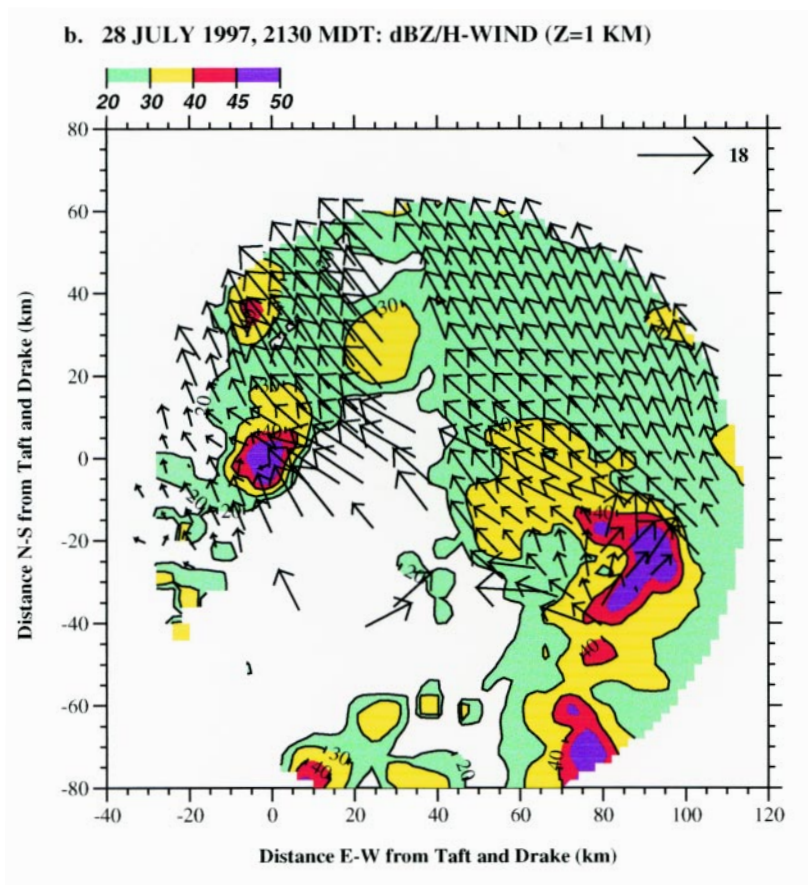

FIG. 12. Dual-Doppler–derived horizontal wind vectors (m s^{-1}) and radar reflectivity (shaded) for the 1-km height level at (a) 2110 MDT 28 July 1997 and (b) 2130 MDT 28 July 1997. Grid origin as in Fig. 9. Vector scale (m s^{-1}) is indicated in the upper-right corner.

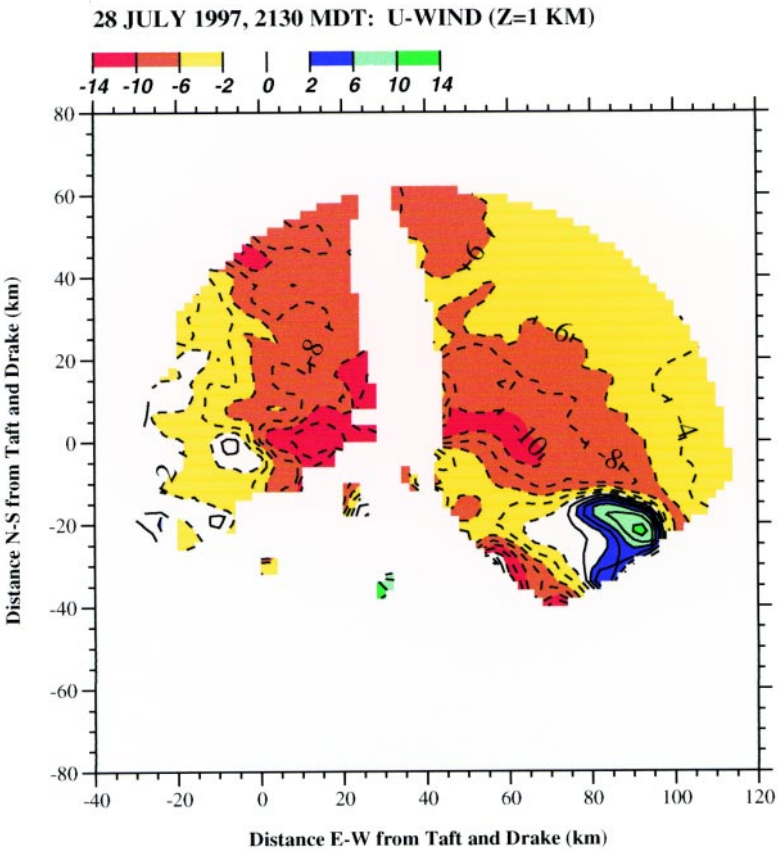

FIG. 13. Dual-Doppler–derived *u*-wind component (shaded) for the 1-km height level at 2130 MDT 28 July 1997. Positive (negative) values of *u* are contoured every 2 m s^{-1} using a solid (dashed) line. Grid origin as in Fig. 9.

several individual cells embedded within the broader envelope of these pulses (e.g., minutes 25, 120, 240) can be summarized as follows.

1) t = 0 min: Development of radar echo below the 3.5–4-km level (≥ 0°C).
2) t = 10–20 min: Peak in echo-top elevation between 9 and 13 km. In the minute 120 and 240 rainfall pulses, CG lightning (albeit infrequent) occurred with penetration of 30–35 dB*Z* mean reflectivities (maximum reflectivities ≥ 40 dB*Z*) into regions of the cloud colder than −10°C. The occurrence of larger reflectivity in the cold region of the cloud is indicative of a more vigorous updraft and a more robust ice process, both of which are conducive to enhanced electrification processes (e.g., Saunders 1995; Williams 1995).
3) t = 25–40 min: Descent of the echo "core," peak in the surface rain mass flux, and continued CG lightning (minutes 120, 240).
4) t = 40–60 min: Rainfall begins to decrease. CG lightning ceases.

One interesting characteristic of the convection was the marked reduction in lightning activity[5] as compared to that of convection located 40–80 km southeast of FCL (e.g., the bow echo system; Fig. 11). For example, the *peak* in CG lightning activity for the FCL event occurred between 1930 and 2015 MDT (minutes 120–165, Fig. 15), yet CG flash rates were only 0.5 flashes per minute. Conversely, peak CG flash rates of 3–4 per minute were typical of the cells located southeast and east of FCL in Fig. 11. During the heaviest rainfall of the evening (2125–2205 MDT, minutes 240–280 in Fig. 15), only 5 CG flashes occurred over a 40-min time period. The relative reduction in CG lightning activity, coincident heavy convective rainfall, and observed thermodynamic structure of the troposphere (Fig. 6; section 4c) suggest the presence of a rainfall process similar to that characteristic of tropical environments (e.g., Rutledge et al. 1992; Williams et al. 1992; Zipser and Lutz 1994; Zipser 1994; Petersen et al. 1996; Petersen et al. 1999).

Indeed, the mean vertical structure of reflectivity associated with the flood convection (Fig. 16) bears some resemblance to that observed in tropical monsoon–oceanic convection (cf. Szoke and Zipser 1986; Williams et al. 1992; Zipser and Lutz 1994; DeMott and Rutledge 1998). For example, in Fig. 15, although echo tops often exceeded 12 km, mean reflectivities > 35 dB*Z* were generally located near or below the height of the −10°C level (5.5 km). The decrease in the normalized vertical *gradient* of radar reflectivity at temperatures lower than 0°C (Fig. 16) in the FCL case is similar to that reported for convective cores over the tropical Atlantic Ocean during the Global Atmospheric Research Program (GARP) Atlantic Tropical Experiment (GATE) (e.g., Szoke and Zipser 1986) and only slightly smaller than that observed over the western Pacific during TOGA COARE (DeMott and Rutledge 1998). As in the tropi-

[5]In addition to the small number of CG flashes detected by the NLDN, a multitude of observers in FCL noted a distinct lack of lightning and thunder after sunset during the period of heaviest rainfall.

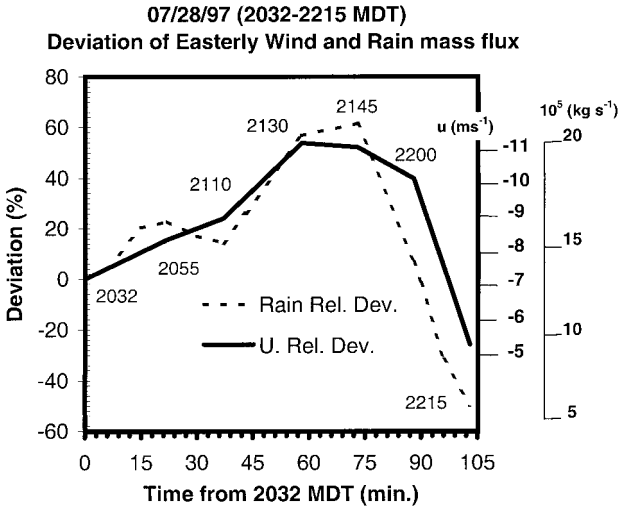

FIG. 14. Time series of the relative deviation (%) of the mean easterly wind component and rain mass flux, from values computed at 2032 MDT (left ordinate). Actual values of easterly wind speed and rain mass flux are indicated on the right ordinate (m s^{-1} and kg s^{-1}, respectively).

cal cases, the low-level convective echo centroid in the FCL case coupled with a large gradient in reflectivity above 0°C likely suggests that warm-rain/collision–coalescence was an important rainfall production mechanism relative to ice-based processes, more commonly associated with precipitation production in high plains thunderstorms (e.g., Dye et al. 1974; Dye et al. 1986; Knight et al. 1974; Heymsfield et al. 1979).

Though heavy rainfall occurred in cells producing little or no lightning during the FCL event, when pulses in the convection extended mean (maximum) reflectivities of ≈35 dB*Z* (40 dB*Z*) to temperatures colder than –10°C (indicative of enhanced mixed phase microphysics and therefore electrification processes; e.g., Williams 1995), CG lightning occurred shortly thereafter (Fig. 15). These observations are consistent with previous studies of lightning-producing convection observed over tropical continents and oceans (Rutledge et al. 1992; Williams et al. 1992; Zipser and Lutz 1994; Petersen et al. 1996; Petersen et al. 1999) and, in the case of maximum reflectivities (not shown), also consistent with electrification onset thresholds observed in New Mexico convection by Dye et al. (1989).

Microphysical characteristics, especially those related to the rainfall process, can be further discerned by examining vertical cross sections (Figs. 17a,b; 2108 MDT) of the polarimetric and radial velocity fields. The northwest to southeast cross sections shown in Figs. 17a–c are representative samples of convective core reflectivities, radial velocity Z_{DR}, and K_{DP} observed by the CSU–CHILL radar along a 295° radial (parallel to the low-level flow) during development of the final, heaviest episode of rainfall (Fig. 15). The highest elevation angle in the CSU–CHILL volume scans never exceeded 9°, hence echo tops above ~8 km were not sampled by the CSU–CHILL radar. The KCYS–NEXRAD volume scan measured an echo top of approximately 13 km near this time located approximately 5–10 km northeast of the storm core.

First note that the diameter of the heaviest raining portion of the convective core (48–51 dB*Z*) in Fig. 17a was only 1 km wide, a characteristic common to the convective cores of the final rainfall pulse in this event. Peak reflectivities in the cell were 57 dB*Z* and were

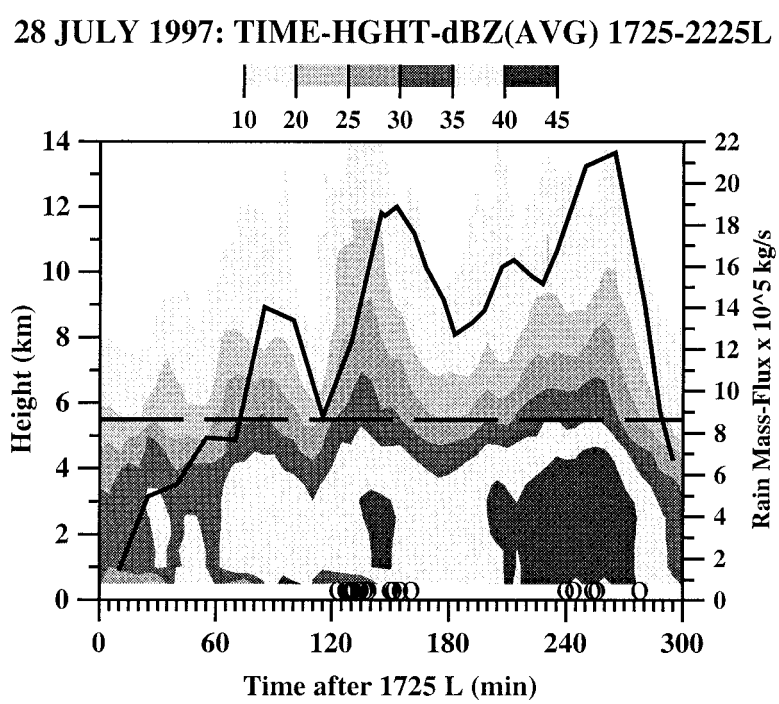

FIG. 15. Time–height series of mean reflectivity (KCYS) for 1725–2225 MDT 28 July 1997. Height (km) is plotted on the left ordinate, time (minutes after 1725 MDT) on the abscissa. A time series of rain mass flux (10^5 kg s^{-1}; bold solid line) [CSU–CHILL blended $R(K_{DP}, Z_{DR})$ estimate; see text] is plotted on the right ordinate. Marks (O) are placed along the abscissa to indicate relative times of CG flash occurrence in the analysis volume. The approximate height of the –10°C level is indicated by a bold dashed line at the 5.5-km height level.

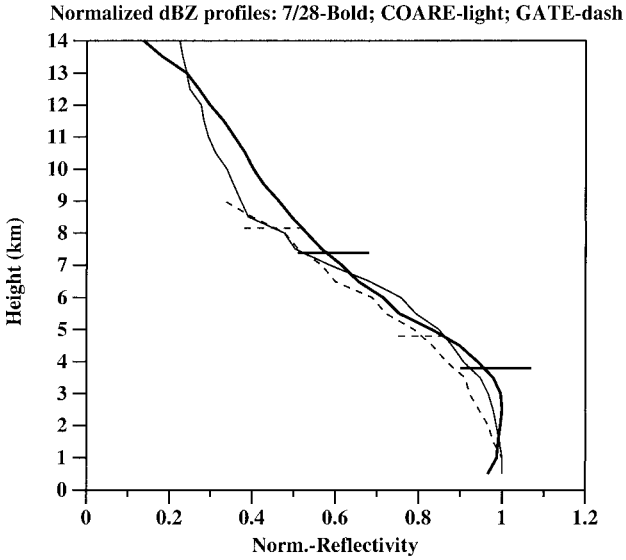

FIG. 16. Height profiles of normalized radar reflectivity (normalized to profile maxima) for the FCL case (bold, solid line), and the mean convective profiles from the TOGA COARE (light, solid; DeMott and Rutledge 1998) and GATE (dashed; Szoke and Zipser 1986) tropical oceanic regimes. Short solid horizontal (dash) lines indicate the heights of the 0° and –20°C temperature levels for the (tropical oceanic) FCL environment.

situated near and just above the height of the 0°C level. Reflectivities of 35 dBZ extended to temperatures colder than –10°C at this time, with the first detected CG lightning occurring 15 min later. Cross sections of Z_{DR} and K_{DP} in Fig. 17a combined with the cross section of radial velocity in Fig. 17b suggest that 2–3-mm diameter raindrops (Z_{DR}'s approaching 2 dB, with K_{DP}'s of 2.5° km^{-1}; e.g., Bringi et al. 1996) were being formed between the 2- and 3-km levels (x = 1 km, Fig. 17b) in the updraft located on the eastern edge of the convective core (x = 0.5–1.5). The vertical extent of Z_{DR} values > 1 dB and K_{DP} values > 1° km^{-1} also suggests that millimeter-sized raindrops were being lofted by the updraft to temperatures colder than 0°C, followed by freezing (Bringi et al. 1996), as indicated by reflectivities near 50 dBZ in the updraft and a rapid falloff in the Z_{DR} and K_{DP} above the 4-km level. To investigate this drop freezing process further, we calculated the reflectivity-weighted ice fraction (f_i) using Z_H and Z_{DR} as outlined in Carey and Rutledge (1996). As shown in Fig. 17c, f_i increased from 0.1 to 0.5 just above the 4-km level in the updraft. However, mixed-phase precipitation existed up to at least 5 km as indicated by the 0.9 ice fraction line (and hence 0.1 rain fraction). This observation is further supported by the presence of an "LDR cap" of –23 to –24 dB overlapping the top of the Z_{DR} core, consistent with drop freezing in a mixed-phase environment (e.g., Bringi et al. 1996; Bringi et al. 1997; Jameson et al. 1996).

The raindrops were lofted through the freezing level along a northwestward trajectory and as they froze likely underwent substantial accretional growth prior to descending on the northwest side of the convective core. The location of the 57 dBZ reflectivity core near and just above the 3.8-km level, situated in horizontal gradients of radial velocity, Z_{DR} and K_{DP}, suggests that the descending ice particles were likely growing by accretion before they melted. Microphysically, the observations for the FCL case seem conceptually similar to that of an "accumulation zone" model of precipitation production. This concept, which involves efficient precipitation production through a coupling of warm-rain and ice-particle accretion processes, has been previously invoked to explain hail growth (e.g., Sulakvelidze et al. 1967) and microphysical observations of rainfall production in tropical cumulonimbi (e.g., Takahashi 1990; Takahashi and Kuhara 1993). A similar microphysical process was proposed by Bringi et al. (1996) in their multiparameter radar study of a storm that produced heavy rain, hail, and minor flooding in Fort Collins in June 1992.

A horizontal cross section of Z_H, Z_{DR}, and K_{DP} at 1.2 km AGL (Fig. 18a) during the time corresponding to Figs. 17a–c reveals interesting microphysical structure that is relevant to the radar estimation of rainfall (Fig. 18b). Cells of high reflectivity exceeding 50 dBZ were approximately collocated with cores of elevated Z_{DR} > 1.5 dB, suggesting the presence of drops in excess of 3 mm (Herzegh and Jameson 1992). Comparison of Figs. 17b and 18a reveals that these cells containing large raindrops, likely resulting from a collision–coalescence process, were located in the updraft along the leading edge of the convective complex. In contrast, the largest values of K_{DP} (≥ 1.5° km^{-1}) were centered primarily in the downdraft and furthermore were displaced to the northwest of the peak values of Z_H and Z_{DR} in the updraft by 1–4 km. This juxtaposition between maxima in K_{DP} and Z_H/Z_{DR} has important implications for storm microphysics and the radar estimation of rainfall, as further discussed below.

The corresponding horizontal cross section of radar-derived rainfall rate is presented in Fig. 18b. We utilize the NEXRAD *Z–R* and a blended $R(K_{DP}, Z_{DR})/Z$–*R* algorithm utilizing CSU–CHILL polarmetric data (cf. section 7d). The blended $R(K_{DP}, Z_{DR})$ estimate produced peak rain rates of 110 mm h^{-1}, while the peak rain rate from the *Z–R* alone is only 75 mm h^{-1}. In addition, the region of heavy rain (R > 50 mm h^{-1}) is sig-

nificantly larger for the $R(K_{DP}, Z_{DR})$ product compared to the Z–R. As expected from Fig. 18a, the peak rain rate from the blended polarimetric algorithm is located in the downdraft several kilometers to the northwest of the peak Z–R.

As discussed in Jameson (1985), $K_{DP} \sim W(1 - \Sigma)$ where W is rain mass mixing ratio and Σ is the mass-weighted rain drop axis ratio. Note that the value of K_{DP} at the peak $R(K_{DP}, Z_{DR})$ in Fig. 18b is only slightly higher than at the peak Z–R. However, Z_{DR} is at least 0.5 dB less at the peak $R(K_{DP}, Z_{DR})$. Since $\Sigma \sim [10^{(ZDR/10]^{-(3/7)}}$ (Jameson 1991), the location of the peak $R(K_{DP}, Z_{DR})$ must contain a larger number of smaller drops relative to the location of the maximum Z_H, Z_{DR}. Of course, the Z–R relationship places the peak rain rate at this point. Studies such as Blanchard and Spencer (1970) suggest that in heavy rain the concentration of smaller drops ($D \sim 1$–2 mm) may increase with increasing rain intensity. This behavior of the drop size distribution in heavy rain can result in an underestimation of the peak rain rate estimated by the NEXRAD Z–R (e.g., Smith et al. 1996) and cause errors in the location of the peak Z-inferred rain rates since reflectivity is biased by the presence of large drops. Although we have insufficient high-resolution rain gauge data to prove that the polarimetric rainfall estimate was more accurate in rainfall amount and location at this time, we will demonstrate in the following section that the blended $R(K_{DP}, Z_{DR})$ algorithm did provide a better estimate of storm cumulative precipitation.

d. Radar-estimated rainfall

The reflectivity (Z) data collected by NEXRAD (e.g., KCYS) and CSU–CHILL radars can be converted to rain rate using reflectivity–rainfall (Z–R) relationships (e.g., Battan 1973). Importantly, polarimetric techniques (cf. Doviak and Zrnic 1993) can also be utilized with the CSU–CHILL data. In opera-

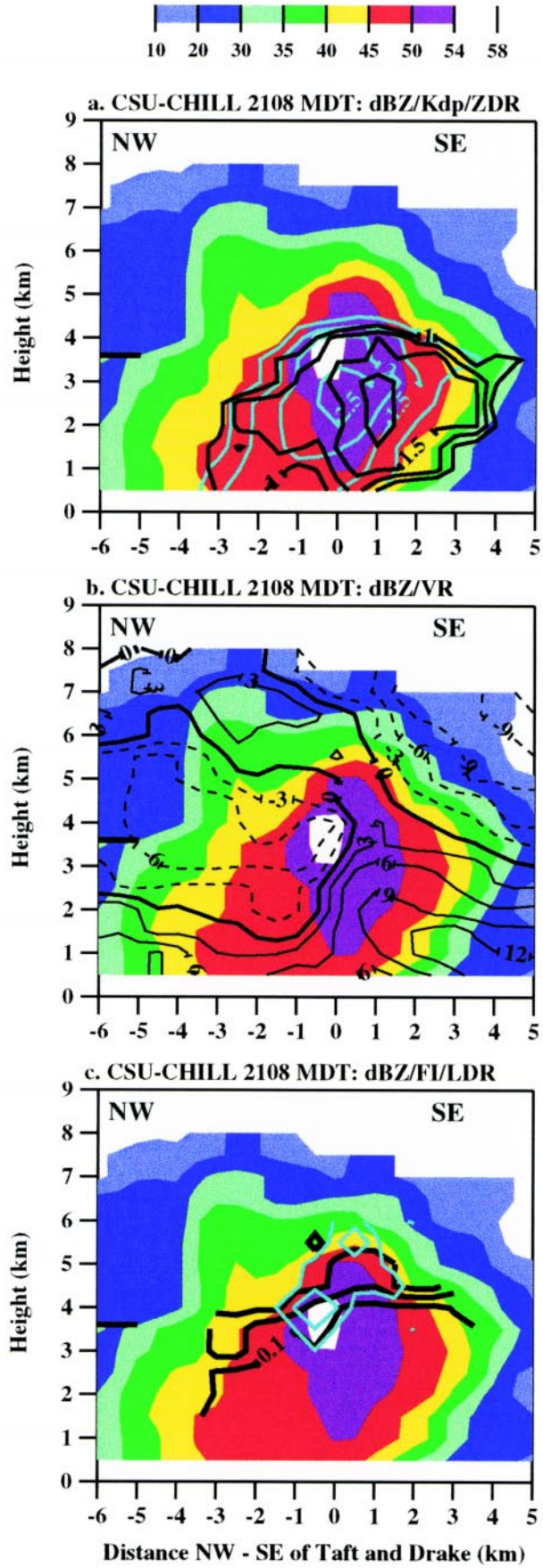

FIG. 17. CSU–CHILL 2108 MDT 28 July 1997. Northwest-southeast cross sections taken along a 295° radial from CSU–CHILL. (a) Reflectivity (shaded), Z_{DR} (black contour), and K_{DP} (light blue contour); contour interval 0.5° km^{-1} (0.25 dB) for K_{DP} (Z_{DR}) starting at 1° km^{-1} (1 dB). (b) Reflectivity and radial velocity; receding (approaching) radial velocities are contoured using solid (dashed) lines at an interval of 3 m s^{-1}. (c) Reflectivity (shaded), precipitation-sized ice fraction (f_i, black contour), and LDR (blue contour). Ice fraction contoured at 0.1, 0.5, and 0.9. LDR contours at –23.5 and –24.5 dB. The approximate height of the 0°C level is indicated by a bold hash mark at Z = 3.6 km. Grid origin as in Fig. 9.

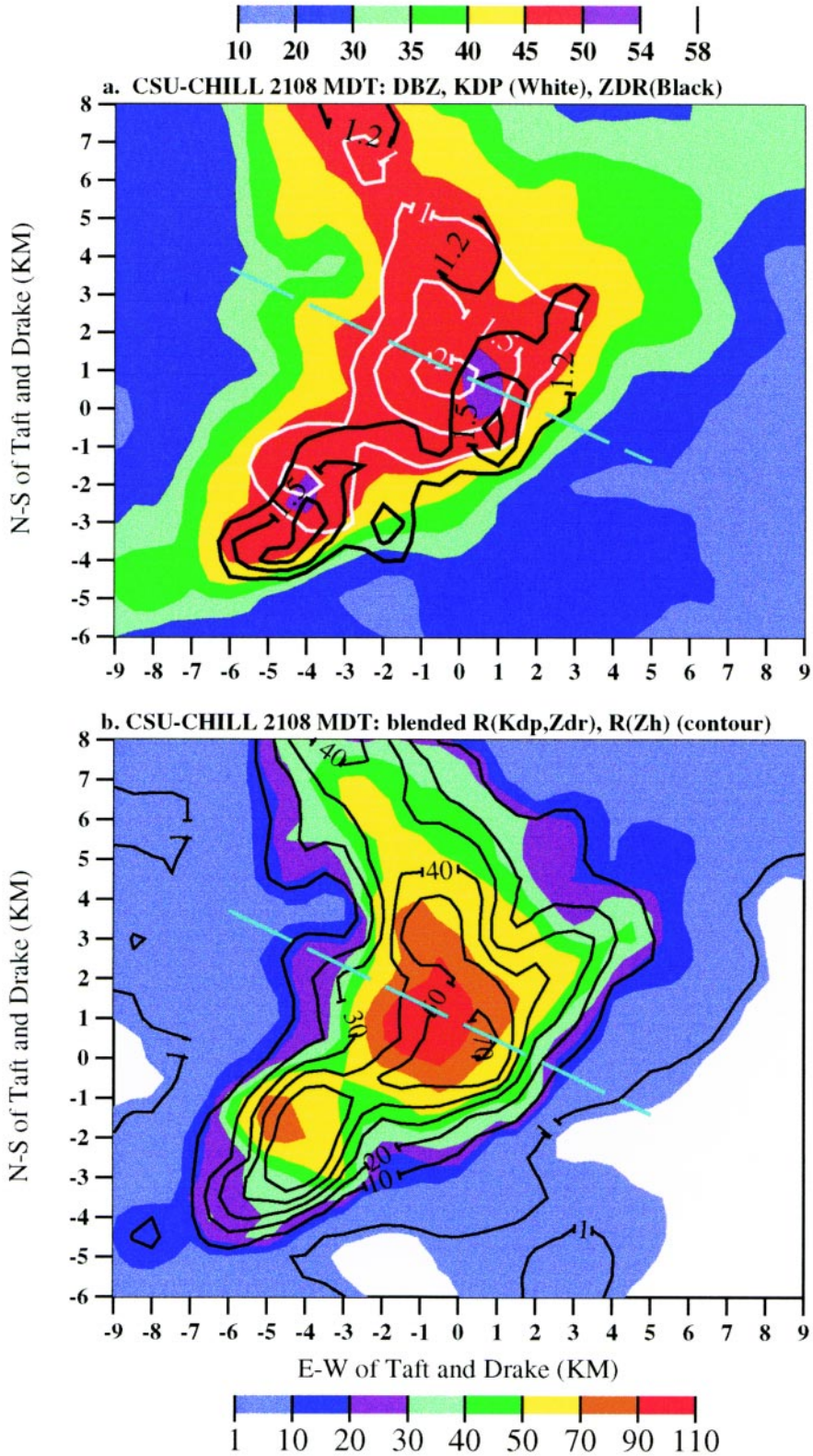

tional settings, especially warning situations, extensive data processing and/or tuning of radar rain-rate relationships in real time is impractical. Therefore it is necessary to examine the relative accuracy of radar–rainfall measurements in postevent processing. Here the word "accuracy" refers to the amount of rainfall measured by the radar compared to that measured by the rain gauge network.

Herein, we briefly discuss several radar estimates of the maximum Storm Total Precipitation (STP) for the FCL flood (Table 2). The rainfall estimates were computed using KCYS Level II reflectivity data, and CSU–CHILL reflectivity and polarimetric data. The data were gridded with a horizontal spacing of 500 m at an elevation of approximately 1 km. Reflectivity-based rain rates were computed for each grid point using the NEXRAD Z–R relationship ($Z = 300R^{1.4}$) applied to both untruncated and truncated reflectivity (53 dBZ) values. Given the apparent tropical nature of the convection, two tropical Z–R relationships (Table 2) were also utilized (Short et al. 1997; Rosenfeld et al. 1993) for comparative purposes. Rain rates were integrated over the 5-h duration of the storm to compute the STP. Level II data from the Denver NEXRAD radar (KFTG) were unavailable during the initial phase of the analysis, though a recent service

FIG. 18. Horizontal cross section at 1.2 km AGL of CSU–CHILL radar data at 2108 MDT 28 July 1997. (a) Reflectivity (shaded), Z_{DR} (black contour), and K_{DP} (white contour). The Z_{DR} is contoured every 0.3 dB starting at 1.2 dB. K_{DP} is contoured every 0.5° km^{-1} starting at 1° km^{-1}. (b) Rainfall rate in mm h^{-1}. The blended $R(K_{DP}, Z_{DR})$ rain-rate product is shaded as shown and the NEXRAD Z–R rain rates are contoured at the same rainfall intensities for direct comparison (1, 10, 20, 30, 40, 50, 70, 90, and 110 mm h^{-1}). The plane of the vertical cross sections shown in Fig. 17 for the same time are indicated by a dashed blue line.

assessment report from the Department of Commerce (NOAA 1997) suggests that the KFTG 6-h STP maximum was on the order of 6 in. (cf. KCYS and CSU–CHILL estimates; Table 2).

In addition to *Z–R* estimates, the CSU–CHILL data permitted a variety of polarimetric rainfall estimates to be computed using multiparameter variables including K_{DP} and Z_{DR} (Doviak and Zrnic 1993; Ryzhkov and Zrnic 1995). For brevity, only the polarimetric estimates of STP computed using combinations of K_{DP} and K_{DR} (Ryzhkov and Zrnic 1995) and K_{DP}, Z_{DR}, and Z (e.g., a "blended product") are shown in Table 2. Theoretically, the use of both K_{DP} and Z_{DR} in the same rain-rate relationship (Table 2) should better account for spatial and temporal variation in the drop size distribution (cf. Ryzhkov and Zrnic 1995).

TABLE 2. Radar rainfall estimates of STP max (1725–2225* MDT).

Radar	Method	STP Max (in.)**
KCYS	*Z–R*: $Z = 300R^{1.4}$	5.0
	Z–R: $Z = 139R^{1.43}$	7.9
	Z–R: $Z = 250R^{1.20}$	10.8
CSU–CHILL	*Z–R*: $Z = 300R^{1.4}$	6.5
	Z–R: $Z = 139R^{1.43}$	10.2
	Z–R: $Z = 250R^{1.20}$	14.9
	$R(K_{DP}, Z_{DR}) = 52\, K_{DP}^{0.96} Z_{DR}^{-0.447}$	8.6
	$R(K_{DP}, Z_{DR})$/*Z–R*	8.0

*1725–2215 for the CSU–CHILL.
**Gauge STP maximum 10 in.

A subjective comparison of radar STP estimates to rain gauge STP was conducted. The criteria for evaluating the various radar techniques relative to the gauges involved a comparison of the location and value of the STP maximum and the overall pattern of the rainfall. The $R(K_{DP}, Z_{DR})$ technique provided the *best match to the gauge STP using an equation previously cited in the literature, with no tuning, and a minimum in processing* (e.g., spurious data and Z_{DR} bias were removed). Two other polarimetric techniques cited in the literature were also utilized [e.g., $R(K_{DP})$, and $R(Z, Z_{DR})$; cf. Doviak and Zrnic 1993] but provided little improvement over the NEXRAD *Z–R* relationship in an absolute sense. Detailed discussion of radar–rainfall measurement using *all* of the potential polarimetric variables/techniques and their application to this case is beyond the scope of this paper but is the subject of several ongoing studies.

Examining the STP estimates in Table 2, the NEXRAD *Z–R* applied to both KCYS (Fig. 19a) and CSU–CHILL reflectivity data produced maximum STPs of 5 and 6.5 in., respectively, only 50%–65% of the gauge total (as was the KFTG estimate; NOAA 1997). Truncation of the reflectivity values to an upper limit of 53 dB*Z*, the maximum reflectivity used in the NEXRAD *Z–R* algorithm, had little effect on the calculated STP. The spatial distribution of the KCYS (Fig. 19a) and CSU–CHILL STPs are broadly consistent with the gauge analysis (Fig. 3b). However, the CSU–CHILL STP maximum was located some 500–1000 m southeast of the KCYS and gauge network STP maxima. The tropical *Z–R* relationships yielded STP distributions and amounts that were similar to the gauge analysis (Fig. 3b). However, the Rosenfeld et al. (1993) *Z–R* relationship produced a marked overestimate (factor of 1.5) of the area-integrated STP relative to the gauge network using CSU–CHILL reflectivity data.

The multiparameter $R(K_{DP}, Z_{DR})$ technique yielded a maximum STP of 8.6 in., approximately 85% of the gauge value, and a spatial distribution of rainfall consistent with that of the gauges (Fig. 3b). Over the entire coverage area, the $R(K_{DP}, Z_{DR})$ estimate was approximately 10%–25% lower than the gauge totals. Though the STP computed from the $R(K_{DP}, Z_{DR})$ relationship was reasonably accurate, several *instantaneous* rain-rate estimates at given grid points over the 5-h duration of the event were contaminated by noisy K_{DP} and Z_{DR} values in regions of moderate to high reflectivity (e.g., 30–50 dB*Z*).

To correct the $R(K_{DP}, Z_{DR})$ rainfall estimates for sampling errors and noise at light to moderate rainfall rates (≤ 15 mm h^{-1}), we created a blended rainfall product that utilized the $R(K_{DP}, Z_{DR})$ estimate in moderate to heavy rain when $Z > 38$ dB*Z*, a linearly weighted $R(K_{DP}, Z_{DR})$/*Z–R* estimate of rain rate in regions of light rain when $35 \leq Z \leq 38$ dB*Z*, and pure *Z–R* estimate in reflectivities < 35 dB*Z* and/or for data points where the K_{DP} or Z_{DR} were below predetermined noise thresholds. The noise thresholds for K_{DP} and Z_{DR} were determined by examining collocated grid points of K_{DP}, Z_{DR}, and *Z*. By visual inspection, the noise thresholds were conservatively determined to be ~0.3° km^{-1} for K_{DP} and ~0.5 dB for Z_{DR}, both thresholds occurring at a reflectivity of 38 dB*Z*. These thresholds are similar to the

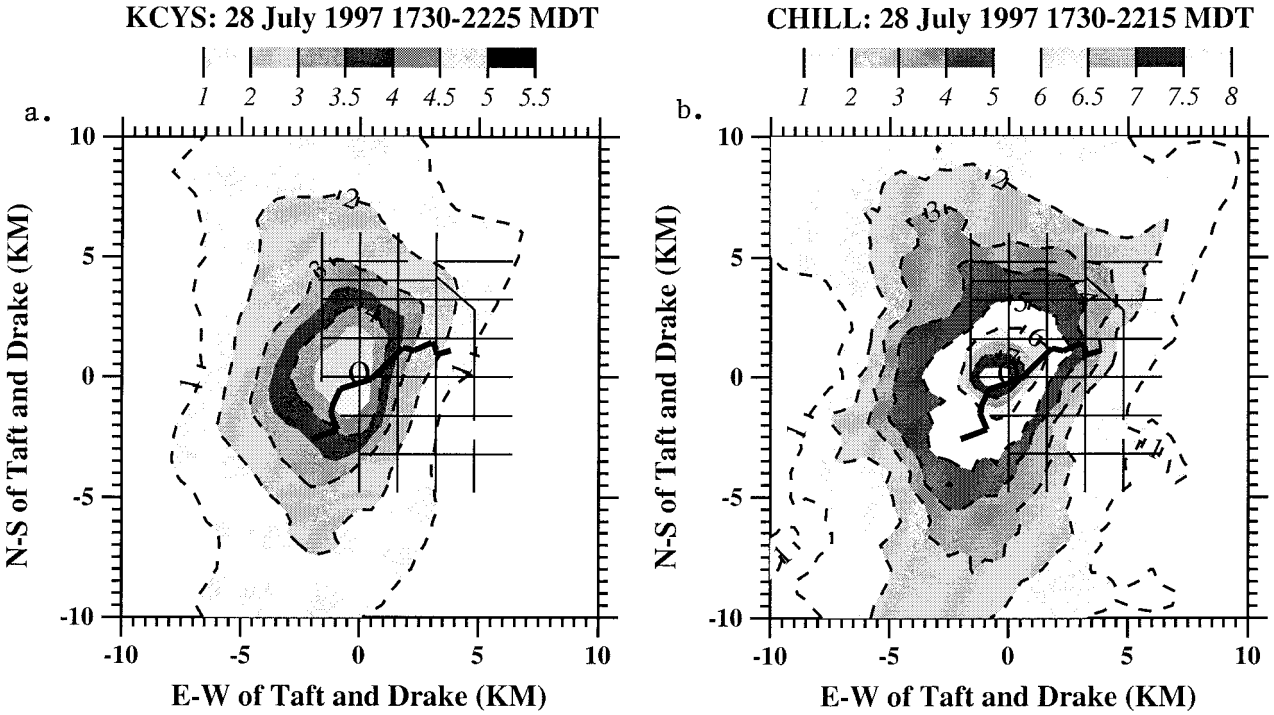

FIG. 19. Storm-total rainfall (in.), 1725–2215 MDT 28 July 1997. (a) NEXRAD *Z–R* estimate using KCYS reflectivity data. (b) CSU–CHILL blended R(K_{DP}, Z_{DR}) estimate. The contour interval in (a) and (b) is 1 in. The origin ("O") is located as in Fig. 9. FCL street grid and location of Spring Creek are also depicted as in Fig. 9. Note the change in scale for shading of rainfall amounts in (a) and (b).

standard errors of the estimators reported in Bringi et al. (1996) for the CSU–CHILL radar. The "tropical" *Z–R* relationships shown in Table 2 (Short et al. 1997; Rosenfeld et al. 1993) were utilized in the blended product (Fig. 19b). Sensitivity tests suggest that the blended product was relatively insensitive to the tropical *Z–R* relationship used and also to small changes (e.g., 0.1° km^{-1}, 0.1 dB, 1 dB*Z*) in the K_{DP}, Z_{DR}, and reflectivity thresholds chosen. Relative to the $R(K_{DP}, Z_{DR})$ estimate, the blended rainfall product (Fig. 19b) exhibited a slight decrease (7%) in the maximum STP, but smoother (spatially) instantaneous rain rates.

In summary, the NEXRAD *Z–R* relationship applied to both KCYS and CSU–CHILL radar reflectivity data produced STP maxima that were only 50%–65% of the gauge STP maximum (similar to underestimates of rainfall by the NEXRAD in the Madison County, Virginia, flash flood of 1995; Smith et al. 1996). While good agreement was attained between gauge-measured STPs and STPs computed using the (Short et al. 1997) Rosenfeld et al. (1993) tropical *Z–R* relationship with the (CSU–CHILL) KCYS NEXRAD data, the relative degree of agreement between the *Z–R*-computed STP and the gauges *was clearly a function of both the radar and relationship used* (Table 2). This is not surprising given the strong functional dependence of *Z–R*-computed rain rates on sampling error, radar calibration, and variations in the drop size distribution (cf. Doviak and Zrnic 1993).

A previously published $R(K_{DP}, Z_{DR})$ relationship applied to the data in both pure and blended forms (e.g., combined with the COARE tropical *Z–R*) provided a reasonable estimate of the STP with minimal tuning (low by a factor of 0.8). It is hypothesized that the combined phase and power information contained in the $R(K_{DP}, Z_{DR})$ estimate better accounted for spatial and temporal variations in the raindrop size distribution (e.g., Ryzhkov and Zrnic 1995).

8. Summary

Extensive meteorological sampling of the environment, convection, and heavy rainfall associated with the Fort Collins flash flood provided key insights into the physical processes responsible for the flood event. From a meteorological perspective the Fort Collins case occurred under the influence of many classic synoptic signatures (e.g., Maddox et al. 1978; Maddox et al. 1980; Caracena et al. 1979; Doswell et al. 1996).

Those signatures included 1) the presence of a negatively tilted 500-hPa ridge over the area and some degree of forcing associated with a weak shortwave trough that moved northward in the western side of the ridge; 2) postfrontal moist easterly upslope flow at low levels; 3) a veering, but weak to moderate, moist, south-southwesterly flow aloft; 4) slow system movement and training convection; and 5) a deep, moist, warm layer in the sounding conducive to precipitation production via warm-rain/collision–coalescence processes. However, unlike the 1976 Big Thompson flood (Caracena et al. 1979), the environment of the Fort Collins flood possessed only modest thermodynamic instability and a lower LFC. This situation led to storm development where the easterly flow encountered its first abrupt lift on the western side of Fort Collins, as opposed to the Big Thompson flood, where parcels required lifting to higher elevations in order to reach the LFC.

Intensive radar sampling coupled with gauge and lightning observations provided a detailed view of the cloud and precipitation morphology. For example, the heaviest convective rainfall occurred in an area on the order of 10×10 km^2; the heaviest precipitation cores were only 1–3 km wide. Relatively little lightning and no hail occurred in association with the storm over Fort Collins, consistent with the presence of only modest thermodynamic instability and the tropical nature of the sounding. Polarimetric radar observations suggest that a coupling between warm-rain/collision–coalescence processes and precipitation ice processes played an important role in the rainfall production associated with the flood convection. Dual-Doppler observations and mesoscale wind analyses revealed that the low-level mesoscale flow field associated with a bow echo may have caused a brief acceleration in the easterly wind component at low levels during the last 1.5 h of the storm. The enhanced easterly flow apparently interacted with convection over Fort Collins, resulting in quasi-stationary convection and heavy rainfall.

Radar estimates of storm total precipitation were computed using the NEXRAD *Z–R* relationship and both CSU–CHILL and KCYS NEXRAD reflectivity data. The resultant NEXRAD *Z–R* estimates of the maximum rainfall accumulation were approximately one-half of that measured by the rain gauge network. Two tropical *Z–R* relationships were also utilized to estimate the storm's accumulated rainfall. Application of the tropical *Z–R*'s yielded a mixed result (e.g., Table 2), as either lower, equal, or higher rainfall totals were produced relative to the rain gauge network *depending on both the radar and the relationship used.* Alternatively, multiparameter radar rainfall estimation techniques such as the $R(K_{DP}, Z_{DR})$ method, which incorporates more information on the temporal and spatial variation of the drop size distribution, provided a reasonable estimate (20% low) of the storm total precipitation with a minimal amount of tuning.

9. Topics for future research

Although sampling of the FCL storms was quite extensive, several questions and topics for further research have arisen out of the analysis conducted thus far and include the following.

1) Radar estimation of rainfall: (a) The NEXRAD *Z–R* relationship provided a significant underestimate of the STP maximum regardless of the radar used. Application of two tropical *Z–R* relationships provided either accurate, excessive, or slight underestimates of the STP maximum depending on the radar and relationship used. Can ancillary meteorological data be used in real time to provide guidance for the selection of an appropriate *Z–R* relationship? If so, over what temporal and spatial scales might this work? To what extent could real-time lightning information be used in this process? (b) While polarimetric techniques such as the $R(K_{DP}, Z_{DR})$ and the blended product yielded reasonable estimates of STP for the FCL flood case with minimal processing, multiparameter techniques such as $R(K_{DP})$ did not appear to work as well. What are the sensitivities of each technique to changes in the assumed drop size distribution, drop shape, and the spatial variability of rainfall? How did the method of calculating K_{DP} (e.g., Hubbert et al. 1993) for *this* case affect the $R(K_{DP})$ and $R(K_{DP}, Z_{DR})$ precipitation estimates?
2) Physical processes: The coexistence of both moving (storms to the south of Fort Collins) and quasi-stationary (the Fort Collins storm) convective systems in the same synoptic environment presents a formidable challenge for forecasting. To what extent did mesoscale processes, topographic effects, interactions between mesoscale convective systems, or other factors, influence the quasi-stationary character of this storm? What factors control whether flash floods along the east slopes of the Rocky Mountains occur at the base of the foothills or farther up in the mountains? The strength of the

upslope flow? The degree of saturation at low levels? Others? Can this distinction be made in flash flood watches? It obviously affects populations that should be taking precautionary measures.

Acknowledgments. This research was supported by the following grants/organizations: NSF/USWRP Grant ATM-9612519, W. A. Petersen, L. D. Carey, and S. A. Rutledge; NSF Grant ATM-9618684, R. H. Johnson, and J. Knievel; Colorado Agricultural Experiment Station, N. J. Doesken and T. B. McKee; NOAA/NESDIS Grant NA67RJ0152, T. Vonder Haar; NOAA/NESDIS Grant NA67RJ0152, J. Weaver. The CSU–CHILL Radar Facility is supported by NSF Grant ATM-9500108 and Colorado State University. We wish to acknowledge the following people for their help: Dr. James Bresch (NCAR), Richard Moore (CSU), Eric Hilgendorf (CIRA), Jim Edwards (FSL), Greg Thompson (NCAR), and Bill Moninger (FSL). Special thanks are extended to Mr. Robert Bowie of the CSU–CHILL Radar Facility who single-handedly operated the CSU–CHILL Radar on the evening of the 28th. Dr. Charles A. Doswell III and two anonymous reviewers are gratefully acknowledged for their helpful comments and suggestions.

References

Battan, L. J., 1973: *Radar Observation of the Atmosphere.* University of Chicago Press, 324 pp.

Bauer-Messmer, B., J. A. Smith, M. L. Baeck, and W. Zhao, 1997: Heavy rainfall: Contrasting two concurrent Great Plains thunderstorms. *Wea. Forecasting,* **12,** 785–798.

Benjamin, S. G., K. A. Brewster, R. Brummer, B. F. Jewett, T. W. Schlatter, T. L. Smith, and P. A. Stamus, 1991; An isentropic three-hour data assimilation system using ACARS aircraft observations. *Mon. Wea. Rev.,* **119,** 888–906.

Blanchard, D. C., and A. T. Spencer, 1970: Experiments on the generation of raindrop-size distributions by drop breakup. *J. Atmos. Sci.,* **27,** 101–108.

Blanchard, D. O., and K. W. Howard, 1986: The Denver hailstorm of 13 June 1984. *Bull. Amer. Meteor. Soc.,* **67,** 1123–1131.

Brady, R. H., and E. J. Szoke, 1989: A case study of nonmesocyclone tornado development in northeast Colorado: Similarities to waterspout formation. *Mon. Wea. Rev.,* **117,** 843–856.

Bringi, V. N., L. Liu, P. C. Kennedy, V. Chandrasekar, and S. A. Rutledge, 1996: Dual multiparameter radar observations of intense convective storms: The 24 June 1992 case study. *Meteor. Atmos. Phys.,* **59,** 3–31.

——, K. Knupp, A. Detwiler, L. Liu, I. J. Caylor, and R. A. Black, 1997: Evolution of a Florida thunderstorm during the Convection and Precipitation/Electrification Experiment: The case of 9 August 1991. *Mon. Wea. Rev.,* **125,** 2131–2160.

Caracena, F., R. A. Maddox, L. R. Hoxit, and C. F. Chappell, 1979: Mesoanalysis of the Big Thompson storm. *Mon. Wea. Rev.,* **107,** 1–17.

Carey, L. C., and S. A. Rutledge, 1996: A multiparameter radar case study of the microphysical and kinematic evolution of a lightning producing storm. *Meteor. Atmos. Phys.,* **59,** 33–64.

——, and ——, 1998: Electrical and multiparameter radar observations of a severe hailstorm. *J. Geophys. Res.,* **103,** 13 979–14 000.

Chappell, C. F., 1986: Quasi-stationary convective events. *Mesoscale Meteorology and Forecasting,* P. S. Ray, Ed., American Meteorological Society, 289–310.

Davis, C. A., 1997: Mesoscale anticyclonic circulations in the lee of the central Rocky Mountains. *Mon. Wea. Rev.,* **125,** 2838–2855.

DeMott, C. A., and S. A. Rutledge, 1998: The vertical structure TOGA COARE convection. Part I: Radar echo distributions. *J. Atmos. Sci.,* **55,** 2730–2747.

Doesken, N. J., and T. B. McKee, 1998: An analysis of rainfall for the July 28, 1997 flood in FCL, Colorado. Climatology Rep. 98-1, Department of Atmospheric Science, Colorado State University, 55 pp. [Available from Colorado Climate Center, Department of Atmospheric Science, Colorado State University, Fort Collins, CO 80523.]

Doswell, C. A., III, 1980: Synoptic-scale environments associated with high plains severe thunderstorms. *Bull. Amer. Meteor. Soc.,* **61,** 1388–1400.

——, H. E. Brooks, and R. A. Maddox, 1996: Flash flood forecasting: An ingredients based methodology. *Wea. Forecasting,* **11,** 560–581.

Doviak, R. J., and D. S. Zrnic, 1993: *Doppler Radar and Weather Observations.* Academic Press, 562 pp.

Dye, J. E., G. Langer, V. Toutenhoofd, and T. W. Cannon, 1974: The mechanism of precipitation formation in northeast Colorado cumulus, III. Coordinated microphysical and radar observations summary. *J. Atmos. Sci.,* **31,** 2152–2159.

——, and Coauthors, 1986: Early electrification and precipitation development in a small, isolated Montana cumulonimbus. *J. Geophys. Res.,* **91,** 1231–1247.

——, W. P. Winn, J. J. Jones, and D. W. Breed, 1989: The electrification of New Mexico thunderstorms I. Relationship between precipitation development and the onset of electrification. *J. Geophys. Res.,* **94,** 8643–8656.

Fujita, T. T., 1978: Manual of downburst identification for project NIMROD. SMRP Research Paper 156, University of Chicago, 42 pp. [Available from Department of Geophysical Sciences, Henry Hinds Laboratory, University of Chicago, 5734 S. Ellis Ave., Chicago, IL 60637.]

Goodman, S. J., D. E. Buechler, P. D. Wright, and W. D. Rust, 1988: Lightning and precipitation history of a microburst-producing storm. *Geophys. Res. Lett.,* **15,** 1185–1188.

Gruntfest, E., 1996: Introduction and overview. What we have learned since the Big Thompson Flood. Special Document 33. Natural Hazard, Research Application Information Center, University of Colorado, 205 pp. [Available from NHRAIC, Campus Box 482, University of Colorado, Boulder, CO 80309-0482.]

Herzegh, P. H., and A. R. Jameson, 1992: Observing precipitation through dual-polarization radar measurements. *Bull. Amer. Meteor. Soc.,* **73,** 1365–1374.

Heymsfield, A. J., C. A. Knight, and J. E. Dye, 1979: Ice initiation in unmixed updraft cores in northeastern Colorado cumulus congestus clouds. *J. Atmos. Sci.,* **36,** 2216–2229.

Holle, R. L., and S. P. Bennett, 1997: Lightning ground flashes associated with summer 1990 flash floods and streamflow in Tucson, Arizona: An exploratory study. *Mon. Wea. Rev.,* **125,** 1526–1536.

Hubbert, J., V. Chandrasekar, and V. N. Bringi, 1993: Processing and interpretation of dual-polarized radar measurements. *J. Atmos. Oceanic Technol.,* **10,** 155–164.

Jameson, A. R., 1985: Microphysical interpretation of multi-parameter radar measurements in rain. Part III: Interpretation and measurement of propagation differential phase shift between orthogonal linear polarizations. *J. Atmos. Sci.,* **42,** 607–614.

——, 1991: A comparison of microwave techniques for measuring rainfall. *J. Appl. Meteor.,* **30,** 32–54.

——, and D. B. Johnson, 1990: Cloud microphysics and radar. *Radar in Meteorology: Battan Memorial and 40th Anniversary Radar Meteorology Conference,* D. Atlas, Ed., American Meteorological Society, 323–347.

——, M. J. Murphy, and E. P. Krider, 1996: Multi-parameter radar observations of isolated Florida cumulonimbi during the onset of electrification. *J. Appl. Meteor.,* **35,** 343–354.

Knight, C. A., N. C. Knight, J. E. Dye, and V. Toutenhoofd, 1974: The mechanism of precipitation formation in northeastern Colorado cumulus, I. Observations of the precipitation itself. *J. Atmos. Sci.,* **31,** 2142–2147.

Maddox, R. A., L. R. Hoxit, C. F. Chappell, and F. Caracena, 1978: Comparison of meteorological aspects of the Big Thompson and Rapid City flash floods. *Mon. Wea. Rev.,* **106,** 375–389.

——, F. Canova, and L. R. Hoxit, 1980: Meteorological characteristics of flash flood events over the western United States. *Mon. Wea. Rev.,* **108,** 1866–1877.

McKee, T. B., and N. J. Doesken, 1997: Final report: Colorado extreme precipitation data study. Climatology Rep. 97-1, Department of Atmospheric Science, Colorado State University, 107 pp. Available from Colorado Climate Center, Department of Atmospheric Science, Colorado State University, Fort Collins, CO 80523.]

Miller, J. F., R. H. Frederick, and R. J. Tracey, 1973: *Precipitation Frequency Atlas of the Western United States.* NOAA Atlas 2, Vol. 3, U.S. Department of Commerce, 67 pp.

Miller, M. J., 1978: The Hampstead storm: A numerical simulation of a quasi-stationary cumulonimbus system. *Quart. J. Roy. Meteor. Soc.,* **104,** 413–427.

Mohr, C. G., and L. J. Miller, 1983: CEDRIC—A software package for Cartesian space editing, synthesis, and display of radar fields under interactive control. Preprints, *21st Conf. on Radar Meteorology,* Edmonton, AB, Canada, Amer. Meteor. Soc., 559–574.

NOAA, 1997: The Fort Collins flash flood. U.S. Department of Commerce, NOAA/NWS, Service Assessment Rep., 23 pp. [Available from NOAA/NWS Office of Hydrology, Silver Spring, MD.]

Petersen, W. A., S. A. Rutledge, and R. E. Orville, 1996: Cloud-to-ground lightning observations from TOGA COARE: Selected results and lightning location algorithms. *Mon. Wea. Rev.,* **124**, 602–620.

——, R. C. Cifelli, S. A. Rutledge, B. S. Ferrier, and B. F. Smull, 1999: Shipborne dual-Doppler operations and observations during TOGA COARE: Integrated observations of storm kinematics and electrification. *Bull. Amer. Meteor. Soc.,* **80,** 81–97.

Przbylinski, R. W., 1995: The bow echo: Observations, numerical simulations, and severe weather detection methods. *Wea. Forecasting,* **10,** 203–218.

Ramachandran, R., A. Detwiler, J. Helsdon Jr., P. L. Smith, and V. N. Bringi, 1996: Precipitation development and electrification of Florida thunderstorm cells during the Convection and Precipitation/Electrification Project. *J. Geophys. Res.,* **101,** 1599–1619.

Rosenfeld, D., D. B. Wolff, and D. Atlas, 1993: General probability matched relations between radar reflectivity and rain rate. *J. Appl. Meteor.,* **32,** 50–72.

Rutledge, S. A., E. R. Williams, and T. D. Keenan, 1992: The Down Under Doppler and Electricity Experiment (DUNDEE): Overview and preliminary results. *Bull. Amer. Meteor. Soc.,* **73,** 3–16.

Ryzhkov, A. V., and D. S. Zrnic, 1995: Comparison of dual-polarization radar estimators of rain. *J. Atmos. Oceanic Technol.,* **12,** 249–256.

Saunders, C. P. R., 1995: Thunderstorm electrification. *Handbook of Atmospheric Electrodynamics,* Hans Volland, Ed., CRC Press, 61–92.

Short, D. A., P. A. Kucera, B. S. Ferrier, J. C. Gerlach, S. A. Rutledge, and O. W. Thiele, 1997: Shipboard radar rainfall patterns within the TOGA COARE IFA. *Bull. Amer. Meteor. Soc.,* **78,** 2817–2836.

Smith, J. A., M. L. Baeck, and M. Steiner, 1996: Catastrophic rainfall from an upslope thunderstorm in the central Appalachians: The Rapidan storm of June 27, 1995. *Water Resour. Res.,* **32,** 3099–3113.

Soula, S., H. Sauvageot, G. Molinie, F. Mesnard, and S. Chauzy, 1998: The CG lightning activity of a storm causing a flash flood. *Geophys. Res. Lett.,* **25,** 1181–1184.

Sulakvelidze, G. K., N. S. Bibilashvili, and V. F. Lapcheva, 1967: *Formation of Precipitation and Modification of Hail Processes.* Isr. Program Sci. Transl., 208 pp.

Szoke, E. J., and E. J. Zipser, 1986: A radar study of convective cells in mesoscale systems in GATE. Part II: Life cycles of convective cells. *J. Atmos. Sci.,* **43,** 199–218.

——, M. L. Weisman, J. M. Brown, F. Caracena, and T. W. Schlatter, 1984: A subsynoptic analysis of the Denver tornadoes of 3 June 1981. *Mon. Wea. Rev.,* **112,** 790–808.

Takahashi, T., 1990: Near absence of lightning in torrential rainfall producing micronesian thunderstorms. *Geophys. Res. Lett.,* **17,** 2381–2384.

——, and K. Kuhara, 1993: Precipitation mechanisms of cumulonimbus clouds at Pohnpei, Micronesia. *J. Meteor. Soc. Japan,* **71,** 21–31.

Weaver, J. F., and N. J. Doesken, 1990: Recurrence probability—A different approach. *Weather,* **45,** 333–339.

——, W. A. Petersen, and N. J. Doesken, 1998: Some unusual aspects of the Fort Collins flash flood of 28 July 1997. Preprints, *Eighth Conf. on Mountain Meteorology,* Flagstaff, AZ, Amer. Meteor. Soc., 3–7.

Weisman, M. L., 1993: The genesis of severe, long-lived bow echoes. *J. Atmos. Sci.,* **50,** 645–670.

——, and C. A. Davis, 1998: Mechanisms for the generation of mesoscale vortices within quasi-linear convective systems. *J. Atmos. Sci.,* **55,** 2603–2622.

Wilczak, J. M., and T. W. Christian, 1990: Case study of an orographically induced mesoscale vortex (Denver Cyclone). *Mon. Wea. Rev.,* **118,** 1082–1102.

Williams, E. R., 1995: Meteorological aspects of thunderstorms. *Handbook of Atmospheric Electrodynamics,* Hans Volland, Ed., CRC Press, 27–60.

——, S. A. Rutledge, S. C. Goetis, N. Renno, E. Rasmussen, and T. Rickenbach, 1992: A radar and electrical study of tropical hot towers. *J. Atmos. Sci.*, **49,** 1386–1395.

Zipser, E. J., 1994: Deep cumulonimbus cloud systems in the tropics with and without lightning. *Mon. Wea. Rev.*, **122,** 1837–1851.

——, and K. R. Lutz, 1994: The vertical profile of radar reflectivity of convective cells: A strong indicator of storm intensity and lightning probability? *Mon. Wea. Rev.*, **122,** 1751–1759.